AIMS Mathematics, 10(3): 7559–7590.
DOI: 10.3934/math.2025348
Received: 27 February 2025
Revised: 22 March 2025
Accepted: 27 March 2025
Published: 31 March 2025

http://www.aimspress.com/journal/Math

Research article

Nonlocal fractional MGT-non-Fourier photothermal model with spatial and temporal nonlocality for controlling the behavior of semiconductor materials with spherical cavities

Mofareh Alhazmi and Ahmed E. Abouelregal*

Mathematics Department, College of Science, Jouf University, P.O. Box 2014, Sakaka, Saudi Arabia

* **Correspondence:** Email: ahabogal@ju.edu.sa.

Abstract: In this work, we present the nonlocal Moore-Gibson-Thompson photothermal (NMGTPT) theory, a novel framework that integrates spatial and temporal nonlocality to address limitations in both traditional and advanced thermoelastic models. Specifically tailored for semiconductor materials with microstructural features, memory effects, and photo-excited phenomena, the NMGTPT theory unifies nonlocal elasticity, MGT thermal relaxation, and photothermal effects to model the complex interplay between heat, deformation, and photo-induced processes. Unlike prior models, the NMGTPT framework incorporates spatial and temporal nonlocalities, enabling the accurate representation of long-range interactions and memory effects. Additionally, the Atangana-Baleanu (AB) fractional operator is integrated into the NMGTPT model to further enhance its ability to describe nonlocal and memory-dependent behavior, making it particularly suitable for advanced material systems. By incorporating a thermal relaxation coefficient, the framework ensures finite-speed thermal wave propagation, effectively addressing the unrealistic prediction of infinite heat speed found in classical models. The theory also integrates photo-excited free carriers, thermal waves, and acoustic waves, proving highly effective in photothermal and photoacoustic studies involving semiconductors. With the inclusion of an internal length scale, the NMGTPT theory successfully captures size-dependent behaviors, which are essential for accurately modeling nanostructured materials, thin films, and composites. This innovation provides a robust platform for investigating the complex dynamics of photothermal and thermoelastic phenomena in advanced material systems.

Keywords: photo-excited phenomena; nanostructured materials; MGT model; fractional operator; spatial and temporal nonlocality

Mathematics Subject Classification: 74A35, 74D10, 74F05, 93D15

1. Introduction

The study of acoustic theories examines how mechanical vibrations propagate through various materials, particularly under the influence of thermoelastic and photothermal effects [1]. These interactions alter the acoustic properties of materials, leading to investigations into the relationships between thermal, mechanical, optical, and acoustic phenomena, particularly in semiconductor and liquid layers [2]. Researchers utilize numerical simulations and analytical models to gain deeper insights into these complex interactions. A significant breakthrough in this field is the use of laser technology to generate ultrafast photoacoustic pulses lasting only nanoseconds. Furthermore, advancements in piezoelectric capacitor sensors have extended the frequency range for detecting weak photoacoustic signals. Notably, mechanical responses produce rapid pressure pulses, whereas thermal processes generate slower ones due to the inherent differences in reaction times between elastic and thermal mechanisms [3]. To further refine the understanding of photoacoustic pulse generation, researchers analyze the governing thermoelasticity equations. By distinguishing between the fast (PA) and slow (PT) mechanical disturbances, a mathematical framework is developed to characterize pulse generation in pulsed mode [4]. This approach improves both the theoretical and practical understanding of photoacoustic phenomena, contributing to advancements in materials research and sensor technology.

When semiconductors are exposed to optical energy, such as laser pulses, free carriers (electrons and holes) are generated within the material. These carriers play a pivotal role in forming acoustic waves through their interaction with the semiconductor's electronic and elastic properties. Photo-generated carriers disrupt the local charge distribution, inducing periodic elastic strain within the material. This strain propagates as an acoustic wave, driven by the strong coupling between the semiconductor's electronic and mechanical behaviors [5]. Additionally, the presence of free carriers can slightly alter the material's elastic constants, though this effect is generally less significant than the strain caused by charge disturbances. These intricate interactions between optical excitation, electronic dynamics, and mechanical wave propagation form the basis of photoacoustic phenomena in semiconductors [6,7]. A thorough understanding of these processes is crucial for optimizing their use in diverse applications, including high-resolution sensing, advanced imaging technologies, and precise material characterization.

Thermoelasticity is a focused area within the broader realm of elasticity theory that investigates how temperature impacts the mechanical behavior of materials. Researchers in this field explore the intricate connections between thermal fields and elastic substances, enabling a deeper understanding of how temperature fluctuations influence stress, strain, and deformation in solids [8]. Such knowledge is critical for the analysis and design of materials and structures that face combined thermal and mechanical challenges. Coupled thermoelasticity advances the study by recognizing the two-way interaction between heat flow and mechanical deformation. In this framework, thermal variations induce stresses and strains through mechanisms such as thermal expansion, while the resulting mechanical deformations, in turn, influence heat distribution within the material [9]. This mutual coupling makes the theory particularly applicable to advanced engineering problems where thermal and mechanical aspects are closely interdependent. Additionally, extended thermoelasticity introduces

more sophisticated considerations, such as finite thermal wave speeds, to address non-Fourier heat conduction and thermal relaxation effects, which account for delays in heat propagation. These factors are crucial for analyzing systems subjected to rapid thermal transients, such as those encountered during laser-material interactions or shock heating [10].

The applications of thermoelasticity extend across fields, highlighting its importance in advanced structural and material design. In aerospace and automotive engineering, the theory aids in analyzing thermal stresses in critical components, such as turbine blades and brake systems, which are subject to extreme temperature gradients [11]. In geomechanics, researchers apply thermoelastic principles to investigate effects in geothermal reservoirs and underground structures, deepening our understanding of subsurface conditions [12]. Moreover, electronic devices benefit from thermoelasticity by providing insights into thermal expansion and stress in semiconductors and microelectronic components—a crucial factor for ensuring their reliability. Finally, in material science, thermoelasticity supports the design of materials with tailored thermal and mechanical properties, including thermoelastic composites and shape-memory alloys, fostering innovations that meet specific performance requirements [13]. Through these diverse applications, thermoelasticity continues to drive significant advancements across multiple disciplines and industries.

In response to the constraints of the classical coupled dynamic theory of thermoelasticity, researchers have developed a variety of extended theories aimed at tackling the intricate challenges of heat conduction and the coupling between thermal and mechanical processes in contemporary engineering and scientific contexts. Notably, the Green–Naghdi (GN) theories [14–16] and the Moore-Gibson-Thompson (MGT) equation [17,18] have emerged as pivotal advancements in the thermoelasticity field.

The Green–Naghdi theories [14–16] were formulated to extend classical thermoelasticity by accounting for the subtleties of energy dissipation. These theories enhance the understanding of heat conduction and thermal stresses within materials, offering comprehensive frameworks that address dynamic thermoelastic problems more effectively. Furthermore, the MGT heat equation [17] has emerged as a pivotal tool in modern thermoelasticity and fluid dynamics. This equation is rooted in a third-order differential framework, which generalizes traditional heat conduction models by incorporating thermal relaxation concepts and higher-order time derivatives. This formulation provides a novel perspective that contrasts with earlier models, particularly the Fourier and Cattaneo–Vernotte heat conduction theories [19,20], by explicitly acknowledging the finite propagation speeds of thermal waves and the effects of thermal inertia. As a result, the MGT equation is particularly well-suited for systems undergoing rapid thermal changes.

Developments in this area have further expanded the application potential of the MGT equation. For instance, Quintanilla has introduced a new heat conduction model within the MGT framework, enhancing its relevance and utility. Additionally, researchers such as Abouelregal et al. [21–24] have modified the MGT-based heat equation by incorporating a relaxation parameter, which extends the GN Type III model. This modification provides a more refined description of energy dissipation and the propagation of thermal waves, particularly when relaxation effects are significant.

The applications of the MGT equation are particularly significant in fluid dynamics, where the interactions between thermal and viscous effects are essential for accurate modeling. Furthermore, it has proven indispensable in micro- and nanoscale heat transfer scenarios, where classical models often fail to capture the complex dynamics of thermal waves at such scales [25,26]. Through these groundbreaking theories and their applications, researchers are advancing the understanding of

thermoelastic behavior, laying the foundation for improved designs and enhanced performance in engineered systems.

The development of thermoelastic models represents a substantial advancement over traditional approaches; however, these new models encounter challenges when addressing materials that exhibit nonlocal interactions and memory-dependent behaviors. Such complexities arise in systems where both spatially nonlocal effects and temporal histories play a significant role in influencing mechanical and thermal responses. Consequently, there is a growing demand for sophisticated modeling techniques capable of accurately capturing the dynamic and intricate nature of these materials.

In traditional continuum mechanics, constitutive equations describe how response variables at a material point depend solely on variables measured at that same point, adhering to the principle of local action. This principle asserts that a material point's state is unaffected by conditions at distant points within the material. However, the significance of length scales becomes crucial in evaluating the validity of this local approach [27]. When a material's external characteristic length, such as structural dimensions or wavelengths, significantly exceeds its internal characteristic length, like atomic spacings or heterogeneity sizes, classical constitutive laws provide reliable predictions. Conversely, when the external and internal length scales are comparable, local theories fail to capture the actual mechanical behavior of the material, necessitating the adoption of nonlocal methods. Nonlocal continuum field theories address this limitation by incorporating long-range interaction forces, wherein a material point's response is influenced by the states of surrounding points, expressed through response functionals [28].

The growing focus on nanoscience and nanotechnology has made nonlocal continuum mechanics indispensable for modeling and optimizing miniaturized smart devices. With applications in engineering, the goal is to develop effective methods to capture size-dependent behavior and design small-scale structures, leveraging nonlocal mechanics as an alternative to computationally intensive atomistic models [29].

Mathematically, nonlocal theories extend conventional constitutive laws by incorporating long-range interactions through internal characteristic lengths. Eringen's integral elasticity theory [30,31] models stress as the convolution of the elastic strain field with an averaging kernel determined by an internal length, resulting in a strain-driven nonlocal framework. While this approach has proven effective in addressing issues such as screw dislocations and surface waves, it has faced challenges in structural applications [32]. Specifically, conflicts between its constitutive law and the necessary equilibrium conditions have led to contradictory outcomes, as highlighted by prior research and subsequently clarified in follow-up studies. Moreover, the concept of spatiotemporal nonlocality is crucial for linking spatial and temporal aspects in modeling. This idea becomes particularly significant in materials where long-range interactions and historical influences are dominant factors [33]. By offering a comprehensive framework for analyzing material responses, spatiotemporal nonlocality facilitates a profound understanding, especially for nanostructured materials, where conventional models frequently fail to capture the full complexity [34].

The importance of these advancements in nonlocal and spatiotemporal models cannot be overstated. They establish a robust foundation for designing materials with tailored properties and significantly enhance the ability to predict complex phenomena such as wave dispersion, thermal relaxation, and stress redistribution within next-generation materials. This progress represents a pivotal milestone in materials science and engineering, enabling the exploration of innovative studies that emphasize the significance of advanced theoretical models in unraveling complex thermal and

mechanical interactions within materials, offering profound contributions to thermoelasticity, viscoelasticity, and their diverse practical applications in engineering and technology. In their study, Abouelregal et al. [35] introduced a modified spatiotemporal nonlocal thermoelasticity theory that incorporates higher-order phase delays. The findings of this study substantially advanced the understanding of material behavior under rapid thermal loading conditions, providing valuable insights for applications in materials science and engineering design.

Furthermore, Abouelregal et al. [36] presented a groundbreaking space-time nonlocal thermo-viscoelastic model that accounted for two-phase lags in heat diffusion. They focused on analyzing heat transfer in a half-space domain subjected to an external heat source. By developing this innovative framework, the authors offered a comprehensive model for understanding the dynamics of heat diffusion and its implications for material behavior under thermal stress, thereby addressing critical challenges in modern materials engineering.

There are several studies that significantly contribute to our understanding of semiconductor behavior under photothermal excitation, addressing critical factors such as moisture effects, nonlocal interactions, and size-dependent phenomena. These investigations are indispensable for advancing semiconductor technology, as they offer a deeper insight into how semiconductors respond to complex environmental and operational conditions. El-Sapa et al. [37] examined photothermal excitation processes in semiconductor materials, specifically considering the impact of moisture diffusivity. Their analysis revealed how moisture alters the thermal and optical properties of semiconductors during photothermal excitation, providing valuable insights into the performance and stability of these materials under real-world conditions. Moreover, El-Sapa et al. [38] studied the application of the Moore-Gibson-Thompson (MGT) theory to a nonlocal excited semiconductor medium. Their work focused on the stability characteristics of the medium under various excitation conditions, offering a profound understanding of how nonlocal effects influence the behavior of semiconductors when subjected to photothermal excitation. Extending this line of inquiry, El-Sapa et al. [39] incorporated the effects of moisture diffusivity into the MGT model for semiconductor materials under photothermal excitation. Through a combination of theoretical frameworks and numerical simulations, they demonstrated how moisture influences the photothermal response of semiconductors. These findings are critical for improving the efficiency and reliability of semiconductor devices, particularly in humid operational environments.

Conventional thermoelastic models, encompassing both classical and extended coupled theories, face significant limitations in accurately capturing nonlocal interactions within materials where long-range effects play a critical role in thermal and mechanical responses. Moreover, these models struggle to account for memory-dependent behavior, where prior states profoundly influence current dynamics, particularly in scenarios involving thermal relaxation and wave propagation. Additionally, local theories often overlook microscopic-scale effects, which are essential in nanostructured and composite materials. This study addresses these critical gaps by proposing a comprehensive theoretical framework that integrates spatiotemporal nonlocality, thermal relaxation, and photothermal coupling, thereby enabling more accurate predictions of material behavior at small scales.

We introduce the Moore-Gibson-Thompson Nonlocal Photothermal (MGTPT) theory, a groundbreaking framework that integrates both spatial and temporal nonlocality to overcome the limitations of traditional and advanced thermoelastic models. This approach is particularly important for materials where microstructural features, memory-dependent behavior, and photo-excited phenomena play pivotal roles. By combining the principles of nonlocal elasticity, MGT thermal

relaxation, and photothermal effects, the MGTPT theory provides a unified and robust framework that captures the intricate interactions among heat transfer, mechanical deformation, and photo-induced processes.

Unlike other models, the proposed framework incorporates nonlocality in both space and time, allowing for the accurate representation of long-range interactions and historical effects. The inclusion of a thermal relaxation coefficient within the Moore-Gibson-Thompson (MGT) equation ensures finite-speed propagation of thermal waves, addressing the unrealistic assumption of infinite heat propagation in classical models. Moreover, the MGTPT theory uniquely integrates the effects of photo-excited free carriers, thermal waves, and acoustic waves, offering a comprehensive and unified description of photothermal and photoacoustic processes, particularly in semiconductors. By introducing an internal length scale, the framework effectively accounts for size-dependent behaviors, which are critical for nanostructured materials, thin films, and composite materials, enabling a more accurate prediction of their mechanical, thermal, and photothermal responses at small scales.

2. Mathematical formulation

In this section, we present the interconnected equations that govern stress, strain, carrier density, and thermal conductivity within nonlocal semiconductors, offering a holistic framework for understanding the intricate interplay among plasma, heat, and elastic waves. These coupled equations will elucidate the dynamics of energy transfer and wave interactions within the semiconductor material, providing a comprehensive and unified model for this complex system.

Constitutive equation for thermoelasticity with electronic deformation [40,41]:

$$\sigma_{ij} = 2\mu e_{ij} + \lambda e_{kk}\delta_{ij} - \gamma\theta\delta_{ij} - \gamma_n N\delta_{ij}. \tag{2.1}$$

The notations in Eq (2.1) are as follows: σ_{ij} represents the stress tensor components, while μ and λ are the Lamé constants describing the material's elasticity. e_{ij} denotes the strain tensor, and e_{kk} measures cubical dilatation (trace of strain tensor). $\gamma = (3\lambda + 2\mu)\alpha_t$ is the strain-temperature coefficient, α_t is the coefficient of linear thermal expansion, and $\theta = T - T_0$ defines the temperature change from a reference temperature T_0. $\gamma_n = (3\lambda + 2\mu)d_n$ refers to the electronic deformation coefficient, d_n is the coefficient of electronic deformation, N represents the carrier density, and δ_{ij} is the Kronecker delta. The strain-displacement relation:

$$e_{ij} = \tfrac{1}{2}\left(u_{i,j} + u_{j,i}\right) \tag{2.2}$$

where u_i denotes the components of the displacement vector. Equation of motion [42]:

$$\sigma_{ij,j} + F_i = \rho\ddot{u}_i \tag{2.3}$$

where F_i represents body force components and ρ Material density. Plasma-thermal-elastic wave equation [43]:

$$D_E\nabla^2 N = \rho\frac{\partial N}{\partial t} + \frac{1}{\tau}N + \kappa\theta + G \tag{2.4}$$

where D_E is the diffusion coefficient for carrier density, describing the rate at which carriers spread within the material. τ represents the carrier lifetime, indicating the average time carriers exist before recombination. κ is the thermal activation parameter, capturing the influence of temperature on carrier

dynamics. G denotes the carrier photogeneration source term, which quantifies the rate at which carriers are generated due to optical excitation.

Energy balance equation for heat conduction [42]:

$$\rho C_E \frac{\partial \theta}{\partial t} + \gamma T_0 \frac{\partial e}{\partial t} = -\nabla \cdot \vec{q} + Q \tag{2.5}$$

where C_E denotes the specific heat at constant volume, $\vec{q}$ represents the heat flux vector, and Q signifies the external heat source.

In semiconductor materials experiencing plasma and photoexcitation, the energy equation gains additional complexity due to the interactions among thermal fields, electronic deformation, and plasma waves. These intricate interactions are fundamental to accurately modeling the energy transfer processes within the material. Consequently, the revised energy equation, which accounts for these factors, is expressed as follows [43]:

$$\rho C_E \frac{\partial \theta}{\partial t} + \gamma T_0 \frac{\partial e}{\partial t} = -\nabla \cdot \vec{q} + Q + \frac{E_g}{\tau} N. \tag{2.6}$$

The supplementary term $E_g N/\tau$ represents the energy impact caused by the generation and recombination of electron-hole pairs resulting from photon absorption when the photon energy exceeds E_g. This term is vital as it quantifies the contribution of these processes to the energy dynamics of the semiconductor, highlighting the critical role of photon absorption in altering the system's energy state.

The heat flux vector, $\vec{q}$, is conventionally defined by Fourier's law, expressed as [44]:

$$\vec{q} = -K \nabla \theta \tag{2.7}$$

where K is the thermal conductivity. However, Fourier's law assumes an infinite speed of heat propagation, which is physically unrealistic, particularly in rapid transient thermal processes or in materials with low thermal conductivity. This shortcoming highlights the need for more sophisticated heat conduction models that account for finite thermal propagation speeds and memory-dependent effects. To address the assumption of infinite thermal propagation speed, the Cattaneo-Vernotte (CV) law incorporates a time-relaxation parameter, τ_0, thereby modifying Fourier's law as [19,20]:

$$\left(1 + \tau_0 \frac{\partial}{\partial t}\right) \vec{q} = -K \nabla \theta. \tag{2.8}$$

The Green-Naghdi (GN) models [15,16] enhance classical thermoelasticity by introducing the concept of thermal displacement, θ_d, which interacts with both the mechanical displacement and the temperature fields. In the GN-III model, the heat flux equation includes an additional thermal displacement gradient term, $K^* \nabla \theta_d$, resulting in the following modified expression [15]:

$$\vec{q} = -K \nabla \theta - K^* \nabla \theta_d \tag{2.9}$$

where K^* represents thermal conductivity rate and thermal displacement satisfies $\dot{\theta}_d = \theta$. Expanding on the CV framework and integrating it with the Fourier law of the third kind (GN-III) involves incorporating memory-dependent effects and interactions that are pivotal to modern thermoelastic models. Within this context, the adjusted GN-III model can be expressed as follows [17,18]:

$$\left(1 + \tau_0 \frac{\partial}{\partial t}\right) \vec{q} = -K \nabla \theta - K^* \nabla T_d. \tag{2.10}$$

To enhance the understanding of memory effects and nonlocal interactions, fractional derivatives

are integrated into heat conduction models. The fractional derivative operator D_t^α (with α within the range of (0,1) broadens traditional heat conduction equations by introducing time-dependent memory effects, which are crucial for materials exhibiting hereditary characteristics.

Thus, the MGT heat equation can be extended by incorporating fractional derivatives, resulting in the following formulation [45,46]:

$$(1 + \tau_0^\alpha D_t^\alpha)\vec{q} = -K\,\nabla\theta - K^*\,\nabla T_d. \tag{2.11}$$

The fractional derivative operator D_t^α can assume various forms depending on the chosen approach, such as the Caputo, Riemann-Liouville, or Grünwald-Letnikov formulations [47,48], as well as the Caputo–Fabrizio (CF) [49] and Atangana–Baleanu (AB) [50] operators. Each of these formulations offers unique methodologies for tackling fractional calculus, providing flexibility in modeling and capturing the intricate behaviors of systems influenced by memory effects and nonlocal interactions.

In this study, we focus solely on the AB fractional operator of degree α, where $\alpha \in (0,1)$. This particular operator is defined as follows [50]:

$${}_0^C D_0^{(\alpha)} Y(t) = \frac{\mathrm{M}(\alpha)}{1-\alpha}\int_0^t \frac{d}{d\mathcal{s}} Y(\mathcal{s}) E_\alpha\left(\frac{\alpha}{1-\alpha}(t-\mathcal{s})^\alpha\right) d\mathcal{s}. \tag{2.12}$$

Here, $\mathrm{M}(\alpha)$ acts as a normalization constant, satisfying the conditions $\mathrm{M}(0) = 1$ and $\mathrm{M}(1) = 1$. By incorporating the fractional derivative-based Eq (2.10) into Eq (2.6), we derive a revised fractional heat conduction equation that effectively accounts for memory effects within the system. This newly formulated equation can be expressed as follows:

$$(1 + \tau_0^\alpha D_t^\alpha)\frac{\partial}{\partial t}\left[\rho C_E \frac{\partial\theta}{\partial t} + T_0\gamma\frac{\partial e}{\partial t} - Q - \frac{E_g}{\tau}\frac{\partial N}{\partial t}\right] = \frac{\partial}{\partial t}\nabla\cdot(K\,\nabla\theta) + \nabla\cdot(K^*\,\nabla\theta). \tag{2.13}$$

In the realm of nonlocal elasticity theory, the standard local stress-strain relationship is extended to incorporate the effects of long-range interactions within a material. Unlike classical elasticity, which assumes that stress at a specific location is influenced solely by the strain at that same location, nonlocal elasticity integrates contributions from neighboring points within the material's domain. The nonlocal stress-strain relation can be mathematically expressed as follows [30,31]:

$$T_{kl}(\boldsymbol{X}) = \int \sigma_{kl}(\boldsymbol{X}')\hbar(|\boldsymbol{X} - \boldsymbol{X}'|, \xi)\mathrm{d}\Omega(\boldsymbol{X}') \tag{2.14}$$

where $T_{kl}(\boldsymbol{X})$ is the nonlocal stress tensor at the position $\boldsymbol{X}$, $\sigma_{kl}(\boldsymbol{X}')$ represents the local stress tensor at a different point $\boldsymbol{X}'$ in the material, $\hbar(|\boldsymbol{X} - \boldsymbol{X}'|, \eta)$ is the nonlocal kernel function that determines the weighting of stress contributions from various spatial locations, ξ is the internal length scale parameter, which introduces size-dependent phenomena into the analysis, and Ω is the material volume over which the integral is computed.

The space-time nonlocal elasticity model represents a pivotal advancement in continuum mechanics, as it incorporates both spatial and temporal dimensions into the stress-strain relationships of materials. This progression addresses the limitations of classical elasticity theories, which often assume that material behavior is purely local and instantaneous [51]. By accounting for long-range interactions (spatial nonlocality) and memory effects (temporal nonlocality), the model provides a more comprehensive understanding of material responses under dynamic, thermal, and mechanical loading conditions.

Inspired by Eringen's nonlocal elasticity model and the Boltzmann superposition integral, modern

nonlocal elasticity incorporates both spatial and temporal dimensions. Stress and strain are represented through convolution integrals, effectively capturing memory effects and spatial interactions. This approach underscores that a material's response is influenced by both its past states and its surrounding regions, providing a more nuanced understanding of phenomena such as wave propagation, heat transfer, and viscoelasticity. Mathematically, these interactions can be expressed as follows [52]:

$$T_{kl}(\boldsymbol{X},t)=\int_{-\infty}^{t}\int_{\Omega}\mathcal{K}(|\boldsymbol{X}-\boldsymbol{X}'|,t-t')\sigma_{kl}(\boldsymbol{X}',t')\mathrm{d}\Omega(\boldsymbol{X}')\mathrm{d}t'. \tag{2.15}$$

In this context, the nonlocal stress tensor $T_{kl}(\boldsymbol{X},t)$ represents the stress at a specific position $\boldsymbol{X}$ and time t, while the local stress $\sigma_{kl}(\boldsymbol{X}',t')$ reflects the stress at a different location $\boldsymbol{X}'$ and an earlier time t'. The function $\mathcal{K}(|\boldsymbol{X}-\boldsymbol{X}'|,t-t')$ serves as the space-time nonlocal kernel, determining how the influences of past and distant material points affect the stress experienced at the reference point $\boldsymbol{X}$ at time t.

Choosing the kernel function $\mathcal{K}(|\boldsymbol{X}-\boldsymbol{X}'|,t-t')$ is crucial for shaping the extent and nature of nonlocal interactions within space-time elasticity models. The kernel must satisfy certain properties to ensure that the influence of distant stress interactions diminishes with increasing spatial and temporal distances, thus maintaining the model's physical plausibility [53]. By meticulously crafting the kernel, it becomes possible to precisely depict how influences wane over distance and time, mirroring the inherent response of materials to stress.

To establish a suitable kernel function formally, we treat it as analogous to a Green's function for a linear differential operator. This relationship can be mathematically expressed as follows [51]:

$$\Delta\{\mathcal{K}(|\boldsymbol{X}-\boldsymbol{X}'|,t-t')\}=\delta(\boldsymbol{X}-\boldsymbol{X}')\delta(t-t'). \tag{2.16}$$

Here, the notation $\delta(\cdot)$ denotes the Dirac delta function and Δ signifies a differential operator that encompasses both spatial and temporal derivatives. This approach positions the kernel function as a solution to a differential equation, ensuring that it accurately captures the nonlocal effects across both temporal and spatial domains.

To simulate space-time nonlocal elasticity, we suggest employing the Klein-Gordon (KG) operator, which effectively captures wave-like characteristics while incorporating both length and time dependencies. Within this framework, the differential operator Δ is articulated as follows [52]:

$$\Delta=1-\xi^2\nabla^2+\eta^2\frac{\partial^2}{\partial t^2}. \tag{2.17}$$

Here, ξ represents the internal length scale parameter, which regulates spatial nonlocality and addresses effects that vary with size. Moreover, η denotes the characteristic time scale, which embodies temporal nonlocality and encompasses aspects related to memory effects. Together, these parameters play a pivotal role in shaping the behavior of materials under the framework of space-time nonlocal elasticity.

Utilizing the KG operator Δ to the nonlocal stress tensor $T_{kl}(\boldsymbol{X},t)$, we can derive the constitutive equations for isotropic materials within the framework of KG-type nonlocal elasticity as

$$\left(1-\xi^2\nabla^2+\eta^2\frac{\partial^2}{\partial t^2}\right)T_{ij}=\sigma_{ij}=2\mu e_{ij}+\lambda e_{kk}\delta_{ij}-\gamma\theta\delta_{ij}-\gamma_n N\delta_{ij}. \tag{2.18}$$

By applying Eq (2.4) to Eq (2.13), the equation of motion, in the absence of body forces, can be reformulated as:

$$\mu u_{i,jj} + (\lambda + \mu)u_{j,ij} - \gamma\theta_{,i} - \gamma_n N_{,i} = \rho\left(1 - \xi^2\nabla^2 + \eta^2\frac{\partial^2}{\partial t^2}\right)\frac{\partial^2 u_i}{\partial t^2}. \tag{2.19}$$

3. Statement of the problem

In this study, the thermal and mechanical responses of an infinite, isotropic, and homogeneous semiconductor medium with perfect electrical conductivity is analyzed. The medium contains a spherical cavity of radius R_0, where the inner surface is subjected to time-dependent heating and is free from external forces, as illustrated in Figure 1. Furthermore, no internal heat sources or body forces are present within the structure. Employing a spherical coordinate system (r, Θ, ϕ), the governing equations will be investigated and solved, with all pertinent physical and mechanical variables treated as functions of the radial distance r and time t, consistent with the system's inherent symmetry.

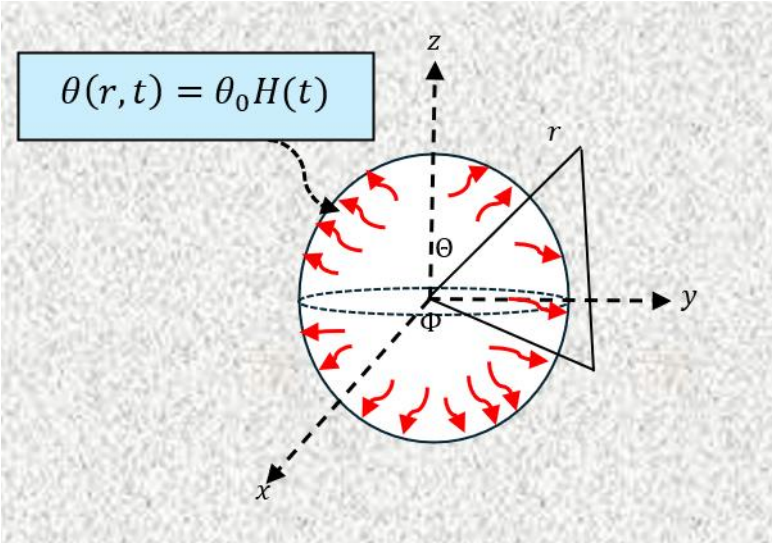

Figure 1. Configuration of the rotating solid semiconductor sphere.

The displacement vector and the displacement-strain relationships within the considered semiconductor medium are described by the following components:

$$\begin{gathered} u_r = u(r,t), \qquad u_\phi(r,t) = 0, u_\Theta(r,t) = 0, \\ e_{rr} = \frac{u}{r}, \qquad e_{\phi\phi} = e_{\Theta\Theta} = \frac{\partial u}{\partial r}, e_{r\phi} = e_{r\Theta} = e_{\phi\Theta} = 0. \end{gathered} \tag{3.1}$$

According to Eq (3.1), the dilatation e is expressed as:

$$e = e_{rr} + e_{\phi\phi} + e_{\Theta\Theta} = \frac{\partial u}{\partial r} + 2\frac{u}{r} = \frac{1}{r^2}\frac{\partial (r^2 u)}{\partial r}. \tag{3.2}$$

The relationships governing stress, strain, temperature, and carrier concentration take the following forms:

$$\left(1 - \xi^2\nabla^2 + \eta^2\frac{\partial^2}{\partial t^2}\right)T_{rr} = \sigma_{rr} = (\lambda + 2\mu)\frac{\partial u}{\partial r} + 2\lambda\frac{u}{r} - (\gamma\theta + \gamma_n N), \tag{3.3}$$

$$\left(1-\xi^2\nabla^2+\eta^2\frac{\partial^2}{\partial t^2}\right)T_{\Theta\Theta}=\sigma_{\Theta\Theta}=\sigma_{\phi\phi}=\lambda\frac{\partial u}{\partial r}+2(\mu+\lambda)\frac{u}{r}-(\gamma\theta+\gamma_n N) \tag{3.4}$$

where $\nabla^2=\frac{1}{r^2}\frac{\partial}{\partial r}\left(r^2\frac{\partial}{\partial r}\right)$.

The dynamic motion equation is expressed as:

$$\frac{\partial T_{rr}}{\partial r}+\frac{2}{r}T_{rr}-\frac{1}{r}\left(T_{\phi\phi}+T_{\Theta\Theta}\right)=\rho\frac{\partial^2 u}{\partial t^2}. \tag{3.5}$$

Incorporating Eqs (3.3) and (3.4) into Eq (3.5) results in:

$$(\lambda+2\mu)\frac{\partial}{\partial r}\left(\frac{1}{r^2}\frac{\partial(r^2u)}{\partial r}\right)-\gamma\frac{\partial\theta}{\partial r}-\gamma_n\frac{\partial N}{\partial r}=\rho\left(1-\xi^2\nabla^2+\eta^2\frac{\partial^2}{\partial t^2}\right)\frac{\partial^2 u}{\partial t^2}. \tag{3.6}$$

By utilizing Eq (3.2), we can reformulate Eq (3.6) to present it in a more concise form:

$$(\lambda+2\mu)\nabla^2 e-\gamma\nabla^2\theta-\gamma_n\nabla^2 N=\rho\left(1-\xi^2\nabla^2+\eta^2\frac{\partial^2}{\partial t^2}\right)\frac{\partial^2 e}{\partial t^2}. \tag{3.7}$$

When there are no heat sources present ($Q=0$), the equation for the generalized fractional modified MGT heat transfer is given by:

$$(1+\tau_0^\alpha D_t^\alpha)\frac{\partial}{\partial t}\left[\rho C_E\frac{\partial\theta}{\partial t}+\gamma T_0\frac{\partial e}{\partial t}-\frac{E_g}{\tau}N\right]=K\nabla^2\dot{\theta}+K^*\nabla^2\theta. \tag{3.8}$$

In the absence of any carrier photogeneration source, the Plasma-thermal-elastic wave equation (1.4) can be expressed as follows:

$$D_E\nabla^2 N=\rho\frac{\partial N}{\partial t}+\frac{1}{\tau}N+\kappa\theta. \tag{3.9}$$

The governing equations can be effectively transformed into dimensionless forms by introducing a set of dimensionless variables, which serve to simplify the analysis. The dimensionless variables are defined as follows:

$$\begin{aligned}&\{r',u'\}=\upsilon_0\delta^*\{r,u\},\{t',\tau_0',\tau',\eta'\}=\upsilon_0^2\delta^*\{t,\tau_0,\tau,\eta\},\theta'=\frac{\gamma}{\rho\upsilon_0^2}\theta,\\&\xi'=\upsilon_0\delta^*\xi,N'=\frac{\gamma_n}{\rho\upsilon_0^2}N,T_{ij}'=\frac{1}{\rho\upsilon_0^2}T_{ij},\delta^*=\frac{\rho C_E}{K},\upsilon_0=\sqrt{\frac{\lambda+2\mu}{\rho}}.\end{aligned} \tag{3.10}$$

If we choose to drop the prime notation, the governing equations can then be rewritten in the following manner:

$$(1+\tau_0^\alpha D_t^\alpha)\frac{\partial}{\partial t}\left[\frac{\partial\theta}{\partial t}+\varepsilon_1\frac{\partial e}{\partial t}-\varepsilon_2 N\right]=\left(\frac{\partial}{\partial t}+\omega^*\right)\nabla^2\theta, \tag{3.11}$$

$$\nabla^2 e-\nabla^2\theta-\nabla^2 N=\left(1-\xi^2\nabla^2+\eta^2\frac{\partial^2}{\partial t^2}\right)\frac{\partial^2 e}{\partial t^2}, \tag{3.12}$$

$$\nabla^2 N=g_1\frac{\partial N}{\partial t}+g_2 N+g_3\theta, \tag{3.13}$$

$$\left(1-\xi^2\nabla^2+\eta^2\frac{\partial^2}{\partial t^2}\right)T_{rr}=\frac{\partial u}{\partial r}+(1-\beta^2)\frac{u}{r}-\theta-N,$$
$$\left(1-\xi^2\nabla^2+\eta^2\frac{\partial^2}{\partial t^2}\right)T_{\Theta\Theta}=(1-\beta^2)\frac{\partial u}{\partial r}+(2-\beta^2)\frac{u}{r}-\theta-N, \tag{3.14}$$

where

$$\beta^2=\frac{2\mu}{\lambda+2\mu},\varepsilon_1=\frac{\gamma^2T_0}{\rho^2C_E\upsilon_0^2},\qquad \omega^*=\frac{K^*}{\upsilon_0^2\rho C_E},\varepsilon_2=\frac{\gamma E_g}{\rho\tau\gamma_{\mathrm{n}}C_E},$$
$$g_1=\frac{\rho}{D_E\delta^*},\qquad g_2=\frac{1}{D_E\delta^*\tau},g_3=\frac{\kappa\gamma_n}{\gamma(\delta^*)^2D_E\upsilon_0^2}. \tag{3.15}$$

4. Initial and boundary conditions of the problem

To solve the system of governing equations and thoroughly characterize the thermoelastic, electronic, and nonlocal properties of the semiconductor medium containing a spherical cavity, the set of initial and boundary conditions is defined as follows:

At the initial time $t=0$, we assume that the medium is initially at rest, i.e.,

$$u(r,t)=0,\frac{\partial u(r,t)}{\partial r}=0,\frac{\partial^2u(r,t)}{\partial t^2}=0,\frac{\partial^3u(r,t)}{\partial t^3}=0,N(r,t)=0,$$
$$T_{ij}(r,t)=0,\frac{\partial T_{ij}(r,t)}{\partial r}=0,\theta(r,t)=0,\frac{\partial\theta(r,t)}{\partial r}=0. \tag{4.1}$$

At the inner surface of the spherical cavity, where $r=R_0$, the medium experiences a rapid application of heat. The thermal boundary condition is expressed as:

$$\theta(R_0,t)=\theta_0H(t),\ t>0 \tag{4.2}$$

where $H(t)$ represents the Heaviside step function and θ_0 is a constant temperature value.

At the inner surface of the spherical cavity, $r=R_0$, nonlocal radial stress is assumed to be zero because of the absence of a traction force. This condition is expressed mathematically as follows:

$$T_{rr}(R_0,t)=0. \tag{4.3}$$

During the diffusion phase, charge carriers have a finite likelihood of recombining as they move toward the sample's surface. This situation results in a flux-type boundary condition for the carrier density that can be described as:

$$D_E\frac{\partial N}{\partial\rho}=s_{\mathrm{v}}N\qquad\text{at}\quad r=R_0 \tag{4.4}$$

Here, s_{v} represents the surface recombination velocity, a metric that quantifies the likelihood of charge carriers recombining at the boundary. The surface recombination velocity (s_{v}) is defined by the equation: $s_{\mathrm{v}}=J/\Delta$, where J represents the recombination current density, which indicates the flux of charge carriers at the surface, and Δn denotes the excess carrier concentration near the surface.

The surface recombination velocity (s_{v}) is a key parameter in semiconductor physics that quantifies the rate at which charge carriers (electrons and holes) recombine at the material's surface or

boundary. It measures the efficiency of the recombination process occurring at the interface, where defects or impurities typically act as recombination centers.

5. Solution in the domain of the Laplace transform

In this section, we explore solutions based on the Laplace transform to illustrate the interactions among thermal, elastic, and plasma waves within nonlocal semiconductors. For a given function $g(r,t)$, the Laplace transform, symbolized by $\mathcal{L}[g(r,t)\,]$ or $\bar{g}(r,s)$, is defined as:

$$\mathcal{L}[g(r,t)\,] = \bar{g}(r,s) = \int_0^\infty g(r,t)\exp(-st)dt, \;\; s > 0. \tag{5.1}$$

Using the Laplace transform on the governing equations (3.11)–(3.14), the following transformed equations are obtained:

$$(\nabla^2 - \psi)\bar{\theta} = \psi\varepsilon_1\bar{e} - \frac{\psi\varepsilon_2}{s}\bar{N}, \tag{5.2}$$

$$\nabla^2\bar{\theta} + \nabla^2\bar{N} = (1 + s^2\xi^2)\nabla^2\bar{e} - s^2(1 + \eta^2 s^2)\bar{e}, \tag{5.3}$$

$$(\nabla^2 - g_4)\bar{N} = g_3\bar{\theta}, \tag{5.4}$$

$$(1 + \eta^2 s^2 - \xi^2\nabla^2)\bar{T}_{rr} = \frac{d\bar{u}}{dr} + (1 - \beta^2)\frac{\bar{u}}{r} - \bar{\theta} - \bar{N}, \tag{5.5}$$

$$(1 + \eta^2 s^2 - \xi^2\nabla^2)\bar{T}_{\Theta\Theta} = (1 - \beta^2)\frac{d\bar{u}}{dr} + (2 - \beta^2)\frac{\bar{u}}{r} - \bar{\theta} - \bar{N}, \tag{5.6}$$

where

$$\psi = \frac{s^2\left(1 + \tau_0^\alpha\,\mathcal{F}(s)\right)}{(\mathrm{s} + \omega^*)}, \mathcal{F}(s) = \frac{s^\alpha}{s^\alpha(1-\alpha) + 1}, g_4 = g_1 s + g_2. \tag{5.7}$$

By separating Eqs (5.2)–(5.4), we obtain a higher-order differential equation that governs the variables $\bar{\theta}$, $\bar{N}$, and $\bar{e}$:

$$(\nabla^6 - q_2\nabla^4 + q_1\nabla^2 - q_0)\{\bar{\theta}, \bar{N}, \bar{e}\} = 0, \tag{5.8}$$

where

$$\begin{gathered} q_2 = \frac{g_4X_2 + X_4}{X_2}, q_1 = \frac{g_4X_4 + X_3\psi - g_3X_5}{X_2}, q_0 = \frac{g_4X_3\psi + g_3X_3X_1}{X_2}, \\ X_0 = \psi\varepsilon_1, X_1 = \frac{\psi\varepsilon_2}{s}, \qquad X_2 = 1 + s^2\xi^2, X_3 = s^2(1 + \eta^2 s^2), \\ X_4 = X_2 + X_3 - X_0, X_5 = X_0 - X_1X_2. \end{gathered} \tag{5.9}$$

Offering p_i (where i =1,2,3) into Eq (5.8) leads us to the expression:

$$(\nabla^2 - p_1^2)(\nabla^2 - p_2^2)(\nabla^2 - p_3^2)\{\bar{e}, \bar{\theta}, \bar{N}\} = 0. \tag{5.10}$$

In this context, p_1^2, p_2^2 , and p_3^2 represent the roots of the polynomial equation:

$$\mathcal{p}^6 - q_2\mathcal{p}^3 + q_1\mathcal{p}^2 - q_0 = 0. \tag{5.11}$$

which can be further detailed as follows:

$$\begin{aligned} \mathcal{p}_1^2 &= \frac{1}{3}[2\mathcal{A}\sin(\mathcal{B}) + q_2], \\ \mathcal{p}_2^2 &= -\frac{1}{3}\mathcal{A}\left[\sin(\mathcal{B}) + \sqrt{3}\cos(\mathcal{B})\right] + \frac{1}{3}q_2, \\ \mathcal{p}_2^2 &= \frac{1}{3}\mathcal{A}\left[\sqrt{3}\cos(\mathcal{B}) - \sin(\mathcal{B})\right] + \frac{1}{3}q_2 \end{aligned} \tag{5.12}$$

where

$$\mathcal{A} = \sqrt{{\alpha_2}^2 - 3\alpha_1},\ \mathcal{B} = \frac{1}{3}\sin^{-1}\left(-\frac{2q_2^3 - 9q_2q_1 + 27q_0}{2\mathcal{B}^3}\right). \tag{5.13}$$

The overall solution to Eq (5.10) can be expressed in the following manner:

$$\{\bar{\theta}, \bar{N}, \bar{e}\} = \frac{1}{\sqrt{r}}\sum_{i=1}^{3}\{1, L_i, H_i\}C_iK_{1/2}(\mathcal{p}_ir). \tag{5.14}$$

The coefficients C_i (with i =1,2,3) are required to be set and depend on s. Furthermore, L_i and M_i are two separate factors linked to C_i. By substituting Eq (5.14) into Eqs (5.2) through (5.4), we arrive at the following relationships:

$$L_i = \frac{g_3}{\mathcal{p}_i^2 - g_4}, \quad H_i = \frac{(\mathcal{p}_i^2 - \psi) - X_1L_i}{X_0},\ \ i = 1,2,3 \tag{5.15}$$

Upon applying the Laplace transform to Eq (3.2) and utilizing Eq (5.14), followed by integration from r to infinity, while assuming that $\bar{u}$ tends toward zero at infinity, we derive:

$$\bar{u} = -\frac{1}{\sqrt{r}}\sum_{i=1}^{3}\frac{H_i}{\mathcal{p}_i}A_iK_{\frac{3}{2}}(\mathcal{p}_ir). \tag{5.16}$$

For large $\mathcal{Y}$, the modified Bessel functions of the second kind, $K_{1/2}(\mathcal{Y})$ and $K_{3/2}(\mathcal{Y})$, exhibit the following asymptotic behavior:

$$K_{1/2}(\mathcal{Y}) \sim \mathrm{e}^{-\mathcal{Y}}\sqrt{\frac{\pi}{2\mathcal{Y}}},\ \ K_{\frac{3}{2}}(\mathcal{Y}) = \mathrm{e}^{-\mathcal{Y}}\sqrt{\frac{\pi}{2\mathcal{Y}}}\left(1 + \frac{1}{\mathcal{Y}}\right). \tag{5.17}$$

When these asymptotic relations are substituted into the general solutions given by Eqs (5.14) and (5.16), the following expressions are derived:

$$\{\bar{\theta}, \bar{N}, \bar{e}\} = \frac{1}{\sqrt{r}}\sum_{i=1}^{3}\{1, L_i, H_i\}C_i\mathrm{e}^{-\mathcal{p}_ir}\sqrt{\frac{\pi}{2\mathcal{p}_ir}}, \tag{5.18}$$

$$\bar{u} = -\frac{1}{\sqrt{r}}\sum_{i=1}^{2}\frac{H_i}{\mathcal{p}_i}C_i\mathrm{e}^{-\mathcal{p}_ir}\sqrt{\frac{\pi}{2\mathcal{p}_ir}}\left(1 + \frac{1}{2\mathcal{p}_ir}\right). \tag{5.19}$$

By inserting the general solutions outlined in Eqs (5.18) and (5.19) into Eqs (5.5) and (5.6), we can deduce that the non-local thermal stresses conform to the following equations:

$$\bar{T}_{rr} = \sqrt{\frac{\pi}{2r}} \sum_{i=1}^{3} \frac{C_i \mathrm{e}^{-\mathscr{p}_i r}\left(-\mathscr{p}_i^2 r^2 (1+L_i) + H_i\left(1+\mathscr{p}_i^2 r^2 + \beta^2 + \mathscr{p}_i r(\beta^2+1)\right)\right)}{(\mathscr{p}_i r)^{5/2}\left(1+\eta^2 s^2 - \xi^2 \mathscr{p}_i^2\right)}, \tag{5.20}$$

$$\bar{T}_{\Theta\Theta} = -\sqrt{\frac{\pi}{2r}} \sum_{i=1}^{3} C_i \frac{\mathrm{e}^{-\mathscr{p}_i r}\left(\mathscr{p}_i^2 r^2\left(1+\mathrm{L}1+H_i(\beta^2-1)\right) + H_i \beta^2 (1+\mathscr{p}_i r)\right)}{(\mathscr{p}_i r)^{5/2}\left(1+\eta^2 s^2 - \xi^2 \mathscr{p}_i^2\right)}. \tag{5.21}$$

The boundary conditions provided in Eqs (4.2)–(4.4) take the following forms after applying the Laplace transform:

$$\bar{\theta}(r, \mathrm{s}) = \frac{\theta_0}{s}, \qquad \text{at} \qquad r = R_0, \tag{5.22}$$

$$\bar{T}_{rr}(r, \mathrm{s}) = 0, \qquad \text{at} \qquad r = R_0, \tag{5.23}$$

$$D_E \frac{\partial \bar{N}}{\partial r} = s_f \bar{N}(R, s) \qquad \text{at} \qquad r = R_0. \tag{5.24}$$

By inserting the general solutions outlined in Eqs (5.18) and (5.20) into Eqs (5.22)–(5.24), we can obtain the following set of equations:

$$\frac{1}{\sqrt{r}} \sum_{i=1}^{3} C_i \mathrm{e}^{-\mathscr{p}_i R_0} \sqrt{\frac{\pi}{2\mathscr{p}_i R_0}} = \frac{\theta_0}{s}, \tag{5.25}$$

$$\sum_{i=1}^{3} \frac{C_i \mathrm{e}^{-\mathscr{p}_i R_0}\left(-\mathscr{p}_i^2 R_0^2 (1+L_i) + H_i\left(1+\mathscr{p}_i^2 R_0^2 + \beta^2 + R_0(\beta^2+1)\right)\right)}{(\mathscr{p}_i)^{5/2}(1+\eta^2 s^2 - \xi^2 \mathscr{p}_i^2)} = 0, \tag{5.26}$$

$$\sum_{i=1}^{3} L_i C_i \mathrm{e}^{-\mathscr{p}_i R_0} \sqrt{\frac{1}{\mathscr{p}_i}} (1 + \mathscr{p}_i R_0) = \frac{s_f}{D_E} \sum_{i=1}^{3} L_i C_i \mathrm{e}^{-\mathscr{p}_i R_0} \sqrt{\frac{1}{\mathscr{p}_i}}. \tag{5.27}$$

We determine the values of the parameters C_i, where i = 1, 2, 3, by solving the system defined by Eqs (5.25) to (5.27).

6. Converting solutions from the Laplace domain to the time domain

The Gaver-Stehfest method, a powerful numerical tool for inverting Laplace transforms, plays a vital role in transitioning solutions from the Laplace domain to the time domain. This method, widely utilized in engineering and applied sciences, offers an efficient and reliable way to compute inverse transforms, especially for functions challenging to invert analytically. To approximate the values of $g(r,t)$ across time intervals, the Gaver-Stehfest method utilizes the following formula [54,55]:

$$g(r,t) \approx \frac{\ln(2)}{t} \sum_{\mathscr{b}=1}^{\ell} \omega_{\mathscr{b}} \bar{g}\left(r, \frac{\mathscr{b}}{t}\ln(2)\right), \mathscr{b} \geq 1, \ t > 0. \tag{6.1}$$

Here, $\omega_{\mathscr{b}}$ represents the coefficients associated with each term in the series expansion, while ℓ indicates the total number of terms included in this expansion (this number must be even). The coefficients $\omega_{\mathscr{b}}$ are exclusively determined by the number of terms in the expansion $\mathscr{b}$ and are defined

as follows [56]:

$$\omega_{\mathscr{b}} = (-1)^{\mathscr{b}+\frac{\ell}{2}} \sum_{\jmath=\frac{\mathscr{b}+1}{2}}^{min\{\mathscr{b},\ell/2\}} \frac{\jmath^{\frac{\ell}{2}}(2\jmath)!}{\left(\frac{\ell}{2}-\jmath\right)!\,(\mathscr{b}-\jmath)!\,(2\jmath-\mathscr{b})!\,(\jmath-1)!\,\jmath!}, \mathscr{b} \geq 1, 1 \leq \ell \leq \mathscr{b} \tag{6.2}$$

The method's efficiency lies in its simplicity and speed, avoiding complex contour integrations and symbolic inversions, thus reducing computational time significantly. Adaptability to a variety of Laplace-transformed functions in fields like heat conduction and fluid dynamics further enhances its utility. For smooth functions devoid of singularities, this method delivers precise results. Despite its advantages, the Gaver-Stehfest method faces challenges such as numerical instability with increasing ℓ values, potentially impacting accuracy. Careful selection of ℓ is crucial to balance precision and stability, ensuring dependable outcomes in the inversion process.

7. Materials and methods

To validate the theoretical findings discussed in earlier sections, we conduct several case studies, presenting numerical values generated using the Mathematica program for the examined physical fields. Furthermore, we verify the proposed model, which incorporates the modified Moore-Gibson-Thompson photothermal (MGTPT) heat equation and accounts for spatiotemporal non-locality. The physical fields under investigation are illustrated through both graphical representations and tables. For the numerical calculations during the theoretical analysis, isotropic silicon (Si) will be selected as the solid semiconductor material. The physical parameters for silicon are provided as follows [57]:

$$\lambda = 3.64 \times 10^{10}\mathrm{Nm}^{-2},\ \mu = 5.46 \times 10^{10}\mathrm{Nm}^{-2},\ \rho = 2330\ \mathrm{kg\,m}^{-3},$$
$$K = 150\ \mathrm{W\,m}^{-1}\mathrm{K}^{-1},\ C_E = 6.95 \times 10^{2}\ \mathrm{J\,kg}^{-1}\ \mathrm{K}^{-1},\ d_n = -9 \times 10^{-31}\ \mathrm{m}^3,$$
$$E_g = 1.11\ \mathrm{eV},\ D_E = 2.5 \times 10^{-3}\ \mathrm{m}^2\ \mathrm{s}^{-1},\ s_f = 2\ \mathrm{m\,s}^{-1},\ \tau = 5 \times 10^{-5}\ \mathrm{s}.$$
$$\alpha_t = 4.14 \times 10^{-6}\mathrm{K}^{-1}, T_0 = 300\mathrm{K}.$$

We analyze the numerical outcomes for a specified time of t = 0.12 and a radius parameter of $R_0 = 1$. These findings have been meticulously examined and are visually displayed in Figures 1 through 6, illustrating the calculated field variables across three scenarios.

7.1. Comparison of fractional derivative operators

In this section, we present a comparative analysis of the numerical results for different fields in an elastic semiconductor medium, concentrating on the effects of the Atangana-Baleanu (AB) and Caputo (C) fractional operators as opposed to the classical scenario with integer-order time derivatives ($\alpha = 1$). By examining the differences and implications of these fractional operators, we aim to gain deeper insights into how they affect the behavior and characteristics of the fields within the semiconductor medium. Our goal is to highlight the distinctive impacts and potential advantages of using fractional operators in analyzing the dynamics of elastic systems governed by fractional derivatives.

In this case study, we investigate how fractional orders influence the behavior of different fields within an elastic semiconductor medium. We analyze three specific fractional orders: $\alpha = 1$ for the conventional model, and $\alpha = 0.85$ and $\alpha = 0.65$ for fractional operators. Our aim is to compare the

numerical results for radial displacement (u), temperature change (θ), nonlocal radial thermal stress (T_{rr}), and carrier density (N) within the spherical cavity of the infinite elastic semiconductor medium across varying radial coordinates (r).

In this section, we explore and compare three variations of the Nonlocal Moore-Gibson-Thompson Photothermal Model (NMGTPT), each customized for specific features and applications. The NMGTPT serves as the baseline framework, utilizing integer-order derivatives with $\alpha = 1$, integrating nonlocal elasticity with finite-speed heat conduction for a conventional yet robust perspective on photothermal processes. The fractional nonlocal NGT photothermal model with Caputo operators (FNMGTPT-C) introduces Caputo fractional derivatives ($0 < \alpha < 1$), which bring in memory effects and account for long-range interactions, enhancing our understanding of thermal and elastic responses over time and distance. Last, the fractional nonlocal MGT photothermal model with AB operators (FNMGTPT-AB) uses AB fractional derivatives, providing a smoother and refined nonlocal response that captures complex dynamics, making it particularly suitable for analyzing intricate photothermal phenomena.

The numerical results for these parameters will be presented in Tables 1–5, providing a structured and clear representation of the variations in their behavior under different fractional orders. This comparative analysis aims to offer insights into how fractional operators, with their varying orders, influence the dynamics and characteristics of the fields studied. By examining the differences in behavior, we seek to enhance our understanding of the role of fractional derivatives in affecting the physical properties of the system.

The numerical results presented in Figure 2 offer a comprehensive examination of temperature variations (θ) within an infinite semiconductor medium containing a spherical cavity under various fractional models. The comparison highlights the impact of fractional derivatives, specifically focusing on the NMGTPT model (α = 1.00), the FNMGTPT-C model with fractional orders of (α = 0.85) and (α = 0.65), and the FNMGTPT-AB model for the same fractional orders.

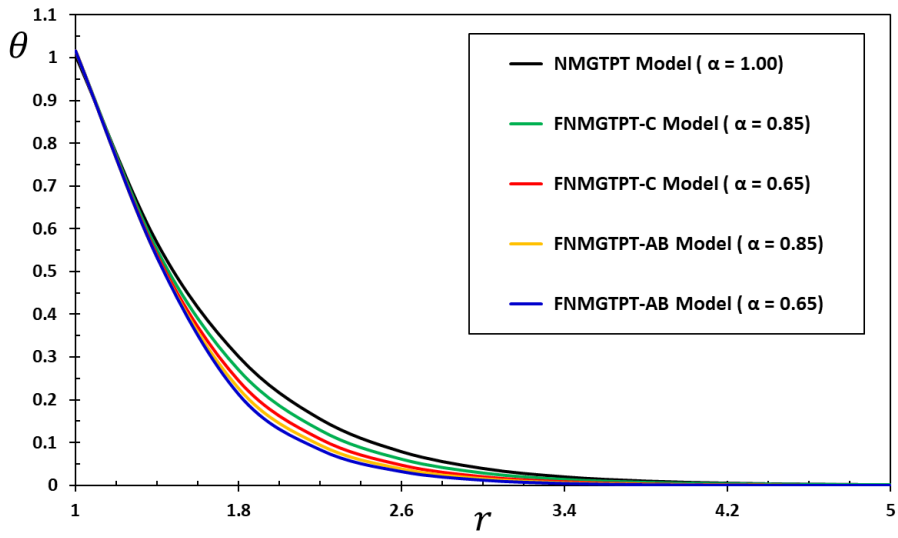

Figure 2. Variation of temperature (θ) across different fractional operators.

Figure 2 highlights that the differences in temperature (θ) between the models become more

pronounced as the radial coordinates (r) increase. At r = 1.4, the NMGTPT model shows a higher temperature of 0.566934 compared to the fractional models. In the case of the FNMGTPT-C model, the temperature drops from 0.550915 (α = 0.85) to 0.539848 (α = 0.65). The FNMGTPT-AB models reflect even lower temperatures, with readings of 0.534157 (α = 0.85) and 0.533669 (α = 0.65). This trend demonstrates that as α decreases, the temperature values also decrease, underscoring the impact of fractional operators. Additionally, the AB operators consistently result in slightly lower temperatures than the C operators, indicating the stronger memory and nonlocal effects associated with the AB formulation.

As r increases, the temperature (θ) decreases more significantly, and the variations among the models become clearer. At r = 3, the NMGTPT model (α = 1.00) produces a temperature of 0.0393976. In comparison, the FNMGTPT-C models yield temperatures of 0.0282343 (α = 0.85) and 0.0209751 (α = 0.65). The FNMGTPT-AB models exhibit even lower temperatures, with values of 0.016073 (α = 0.85) and 0.0126516 (α = 0.65). These results demonstrate that the AB fractional operators consistently lead to lower temperatures than the C operators for the same fractional order. The decrease in temperature with smaller α reflects the growing influence of memory effects and nonlocal interactions in fractional models. This behavior indicates that the AB fractional operators are more effective at capturing these effects, resulting in a more pronounced temperature decline as the radial distance increases.

The graphical results demonstrate that as α decreases, the temperature values drop across all radial positions, emphasizing the heightened memory effects and nonlocal interactions in fractional models, particularly when α is less than 1. The AB fractional operators consistently deliver lower temperatures than the C operators for the same α, reflecting their smoother responses and superior ability to account for nonlocality and memory effects. Additionally, the NMGTPT model (α = 1.00) registers the highest temperatures, underscoring its limitations in addressing the memory effects and nonlocal interactions present in fractional models.

Therefore, based on this analysis, we can conclude that fractional models, particularly those utilizing AB operators, provide a more precise depiction of temperature distribution in semiconductor media exhibiting memory-dependent behavior. This characteristic renders them especially suitable for analyzing complex thermal systems that surpass the limitations of classical models.

The graphical data presented in Figure 3 depict how radial displacement (u) varies in an unbounded semiconductor medium across various fractional models. The models under consideration encompass the nonlocal NMGPT photothermal model at (α =1.00), the fractional nonlocal FNMGPT-C photothermal model with Caputo derivatives for (α =0.85) and (α =0.65), and the fractional nonlocal FNMGPT-AB Photothermal model with AB derivatives for the corresponding fractional orders. The subsequent analysis delves into the radial displacement behavior as a function of the coordinate (r).

From Figure 3, it is evident that displacement (u) decreases as r increases across all models. However, the differences among the models diminish with increasing r. Additionally, the numerical outcomes illustrated in Figure 3 show that the use of fractional operators results in reduced radial displacement (u), with AB operators leading to a more pronounced decrease compared to C operators. This pattern implies that fractional derivatives, particularly AB operators, improve the system's stiffness or resistance to deformation in the vicinity of the spherical gap. These results support the notion that fractional operators, especially those with lower α, introduce significant nonlocal and memory effects that help mitigate deformation. As a result, the medium becomes less prone to displacement as r increases. The enhanced memory effects related to lower α effectively dampen the

medium's response, highlighting the essential role of fractional operators in elucidating the complex dynamics of such systems.

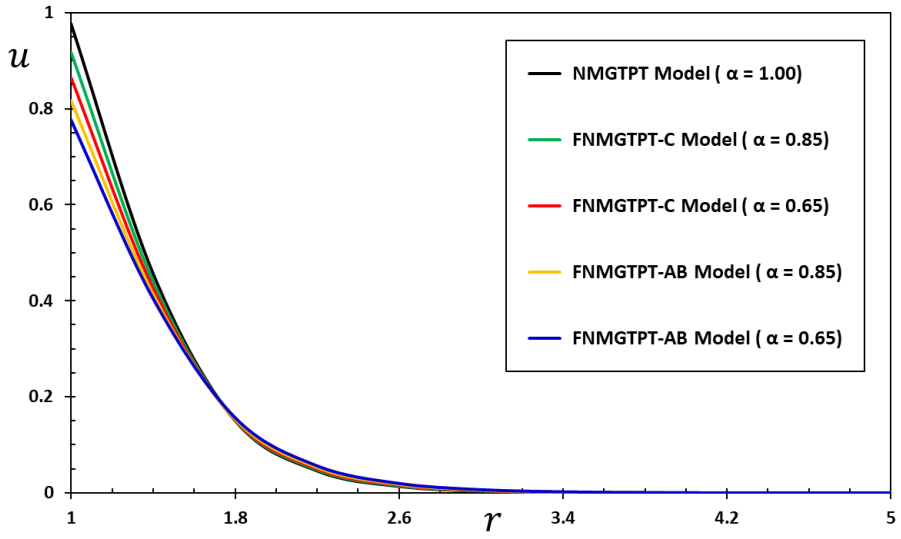

Figure 3. Displacement field (u) across fractional operators.

Analyzing Figure 3 reveals that radial displacement (u) decreases as the fractional order α declines across all radial coordinates. This pattern implies that lower fractional orders strengthen the medium's rigidity and memory effects, thereby reducing its responsiveness to deformation. The enhanced memory effects linked to lower α values allow the medium to resist displacement more efficiently, underscoring the substantial impact of fractional operators on the mechanical behavior of the system. Moreover, AB operators consistently yield lower displacement values than C operators at all radial coordinates. This trend indicates that AB operators provide a more sophisticated framework for modeling nonlocality and memory effects, effectively capturing the complex dynamics of the medium's response. The exceptional capacity of AB operators to incorporate these effects emphasizes their potential for delivering a more accurate portrayal of the medium's behavior under fractional-order formulations.

The results highlight that fractional model, particularly those employing AB fractional operators, offer a more precise description of the medium's behavior by incorporating long-range interactions and memory effects. As a result, these models are particularly advantageous for analyzing advanced materials and systems, where traditional models may fail to capture the intricacies of deformation dynamics.

The numerical findings depicted in Figure 4 reveal the behavior of nonlocal radial thermal stress (T_{rr}) in the semiconductor medium under various fractional differential operators. The comparison between the NMGTPT model (α = 1.00) and the fractional models (FNMGTPT-C and FNMGTPT-AB) for different α values highlight the impact of memory effects and nonlocal interactions on thermal stress distribution. It is observed that at r = 1, all models yield T_{rr}, indicating that the stress is zero at the inner boundary of the semiconductor medium. This suggests that, at this boundary, the effects of fractional operators do not lead to changes in thermal stress.

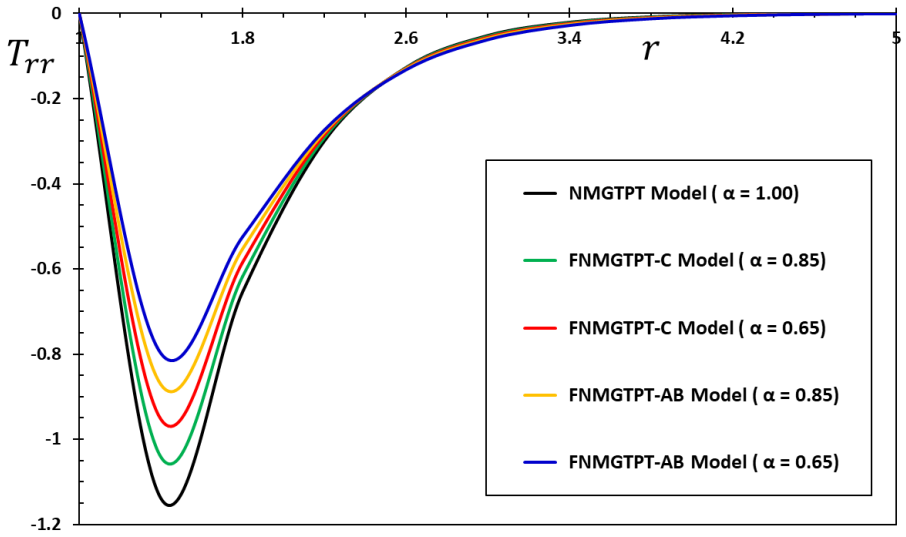

Figure 4. Nonlocal radial thermal stresses (T_{rr}) across different fractional operators.

In Figure 4, it is illustrated that as r increases, the absolute value of T_{rr} decreases across all models; however, clear distinctions arise among them. Specifically, the NMGTPT model ($\alpha = 1.00$) generates the highest compressive thermal stress of $T_{rr} = -1.13917$ at $r = 1.4$. Conversely, the fractional models display progressively smaller stress values. This trend indicates that as α decreases, the influence of memory effects becomes more significant, leading to a reduction in thermal stress. Moreover, the AB operators, which are more responsive to nonlocality, further enhance this decrease in stress.

Figure 4 reveals that the NMGTPT model features the highest thermal stress values, demonstrating the propensity of classical models to overstate stress by overlooking memory effects. As the fractional order α decreases, a clear reduction in thermal stress is noted across all radial positions, emphasizing the growing impact of memory effects and nonlocality in alleviating stress concentrations within the semiconductor medium. Among the fractional operators, the AB operators consistently yield lower stress magnitudes compared to the C operators for the same α, indicating their more effective nonlocal influence. This suggests that AB operators enable a more efficient and gradual stress relaxation in semiconductor materials, offering a significant benefit in accurately representing realistic stress behaviors. Consequently, the results suggest that fractional models, especially those utilizing AB operators, provide a more reliable representation of stress distribution, making them highly relevant for semiconductor applications where effective thermal stress management is crucial.

In Figure 5, the variation in nonlocal hoop thermal stress ($T_{\Theta\Theta}$) within a semiconductor medium is shown, influenced by different fractional differential operators. By examining the values across various radii (r) for the models (NMGTPT (α = 1.00), FNMGTPT-C ($\alpha = 0.85$, $\alpha = 0.65$), and FNMGTPT-AB ($\alpha = 0.85$, $\alpha = 0.65$), we can see how these operators affect thermal stress distribution within the medium. It is observed from Figure 5 that at $r = 1$, the NMGTPT model yields the highest thermal stress of 0.130292. In comparison, the FNMGTPT-C model reduces the stress to 0.12198 for $\alpha = 0.85$ and further to 0.114549 for $\alpha = 0.65$. The FNMGTPT-AB models show even lower values at 0.1021 for $\alpha = 0.85$ and 0.0969979 for $\alpha = 0.65$. This pattern suggests that fractional derivatives effectively lower thermal stress, highlighting their importance in reducing stress under nonlocal conditions. At $r = 1.4$, the trend appears to change, with the NMGTPT model showing a thermal stress

($T_{\Theta\Theta}$) of 0.011188. In contrast, the FNMGTPT-C models exhibit an increase, reaching values of 0.0134008 for α = 0.85 and 0.0154321 for α = 0.65. The FNMGTPT-AB models also follow a similar trend, peaking at 0.0208603 for α = 0.65. This observation indicates a complex relationship in which lower fractional orders enhance the model's sensitivity to thermal stress in this specific range.

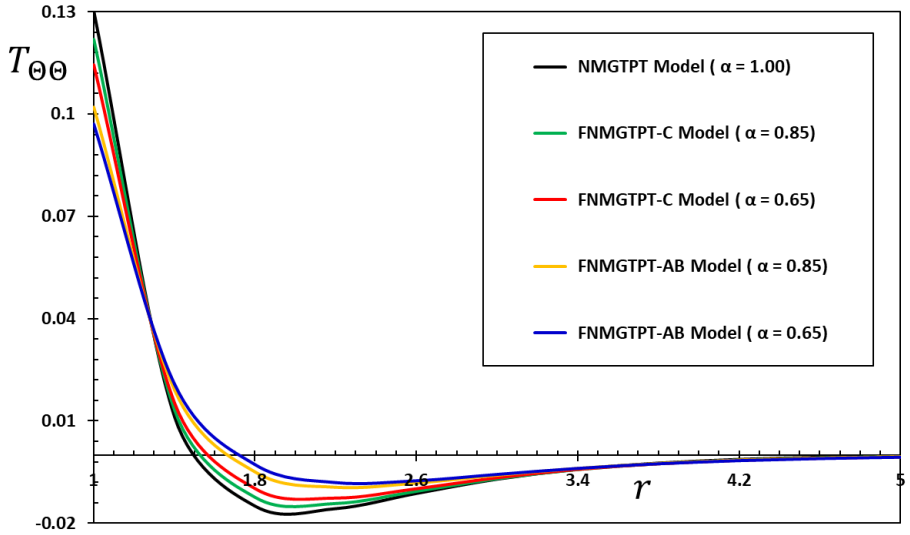

Figure 5. Nonlocal hoop thermal stresses ($T_{\Theta\Theta}$) across fractional operators.

According to Figure 5, beyond r = 1.8, all models, including NMGTPT, begin to produce negative thermal stresses ($T_{\Theta\Theta}$), indicating a transition in the thermal behavior of the medium. For instance, the FNMGTPT-C model records values of -0.0123442 for α = 0.85 and -0.00976649 for α = 0.65, while the FNMGTPT-AB models demonstrate a more gradual decline. This observation highlights the role of fractional derivatives in altering thermal stress behavior, particularly in nonlocal regions. At larger radii (r > 3), the thermal stress values trend toward small negative levels across all models. For example, at r = 5, the NMGTPT model forecasts -0.000425308, whereas the FNMGTPT-AB model with α = 0.65 approaches -0.000624862. This convergence indicates decreasing discrepancies among the models, leading to a more consistent thermal response as distance increases.

The results highlight that fractional differential operators have a profound impact on the distribution of nonlocal hoop thermal stress ($T_{\Theta\Theta}$) in semiconductor materials. Although the NMGTPT model estimates higher localized stress values, fractional models, particularly those using AB fractional operators, reduce these stresses and expose intricate nonlocal interactions that are affected by the value of α. This emphasizes the significance of fractional operators in portraying the detailed thermal behavior of semiconductor media under various conditions.

The numerical results presented in Figure 6 illustrate the variation in carrier density (N) within a semiconductor medium, as influenced by different fractional differential operators. The data is categorized using various models, including the NMGTPT model and the fractional FNMGTPT-C and fractional FNMGTPT-AB Models, with fractional orders of α = 1.00, 0.85, and 0.65. By examining the carrier density (N) across varying radial distances (r), meaningful insights can be drawn regarding the impact of fractional operators on the distribution and retention of carriers within the medium.

From Figure 6, it is observed that at the cavity (r = 1), the NMGTPT model exhibits the highest

carrier density (N) of 0.00210137, while the fractional models demonstrate a significant reduction in carrier density. The FNMGTPT-C model shows a carrier density of 0.00185516 for $\alpha = 0.85$, which further decreases to 0.00162501 for $\alpha = 0.65$. The FNMGTPT-AB models report even lower densities, suggesting that the fractional order has a substantial impact on carrier behavior. This trend implies that fractional operators, particularly the AB operators, introduce nonlocal effects and memory characteristics that contribute to the reduction of carrier density (N) near the origin. The reduction becomes more pronounced as the fractional order decreases, emphasizing the role of fractional derivatives in modifying the dynamics of carrier distribution (N).

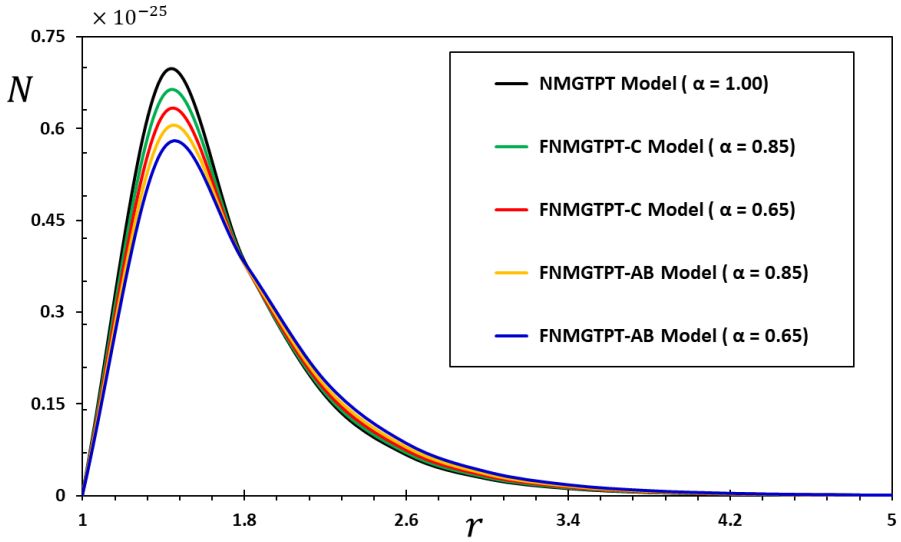

Figure 6. Carrier density (N) across fractional operators.

Figure 6 illustrates that as the radial distance increases, the carrier density (N) decreases across all models, though the rate of this decline differs based on the fractional order and the specific operator applied. At $r = 1.4$, the NMGTPT model indicates a carrier density (N) of 0.688725, while the FNMGTPT-C models show lower values of 0.654672 for $\alpha = 0.85$ and 0.623269 for $\alpha = 0.65$. The FNMGTPT-AB models follow a similar pattern, indicating even lower densities. This behavior signifies that all models project a consistent reduction in carrier density with higher radial distances; however, fractional operators, particularly those with lower fractional orders, exhibit a more substantial impact on decreasing densities (N) at moderate distances. The AB models, in particular, reveal more pronounced nonlocal effects, showcasing their capacity to effectively capture the complexities of carrier dynamics.

At the greater radial distance of $r = 2.6$, the differences in carrier density (N) among the models become less distinct, particularly for the FNMGTPT-C models, which maintain similar values of carrier densities (N). For instance, the NMGTPT model predicts a carrier density (N) of 0.0663637, while the FNMGTPT-C models yield comparable densities, signifying that the influence of fractional order lessens as the radial distance increases. In contrast, the FNMGTPT-AB models consistently report slightly higher carrier densities (N) than their FNMGTPT-C counterparts at the same fractional orders, suggesting that the AB models are more effective at preserving carriers at larger distances. This finding emphasizes the contribution of AB operators to a more gradual and refined decrease in carrier

density (N).

As the radial distance continues to increase, particularly at $r = 5$, carrier densities (N) experience a notable decline across all models. The NMGTPT model reports a carrier density of 0.0003877, while the FNMGTPT-C models persist in their downward trajectory, with the lowest densities found in models featuring the smallest fractional orders. Conversely, the FNMGTPT-AB models show a relatively greater retention of carriers (N), with the model for $\alpha = 0.65$ producing a density of 0.000887086, which is noticeably higher than that of the corresponding FNMGTPT-C model. This trend highlights the effectiveness of AB operators in alleviating the loss of carriers at larger distances, demonstrating their superiority in capturing nonlocal carrier dynamics in semiconductor systems.

In conclusion, the findings from Figure 6 indicate that fractional differential operators play a crucial role in influencing the behavior of carrier density (N) in semiconductor media. The NMGTPT model, while predicting the highest carrier densities near the origin, does not consider the nonlocal and memory effects that are intrinsic to fractional models. The FNMGTPT-C and FNMGTPT-AB models incorporate these effects, leading to reduced carrier densities (N) and showcasing complex interactions that are dependent on the fractional order α. Among these models, the AB operators consistently exhibit superior carrier retention, especially at larger distances, which enhances their suitability for accurately modeling carrier behavior (N) in semiconductor applications. These findings highlight the significance of fractional calculus in furthering the understanding and forecasting of carrier dynamics in complex materials.

7.2. Effects of length and time scale parameters

Many researchers have emphasized the critical importance of the intrinsic length scale (ξ) and time scale (η) in accurately modeling the dynamic behavior of elastic nanomaterials under transient thermal and mechanical loads. Despite this, limited research encompasses their influence on semiconductor materials. By incorporating these parameters, it becomes possible to better account for size-dependent phenomena, time-delayed responses, and nonlocal effects. This integration provides a more precise framework for analyzing semiconductor nanomaterials, offering valuable insights that can enhance their practical applications.

To address this gap, we investigate the thermoelastic and photoelastic responses within an elastic semiconductor medium. Specifically, the study examines the non-dimensional radial displacement field (u), carrier density (N), nonlocal thermal stresses ($T_{\Theta\Theta}$, T_{rr}), and temperature variation (θ). Through this analysis, we aim to elucidate the interplay between these parameters and their influence on the behavior of semiconductor nanomaterials.

Figure 7 illustrates the impact of the intrinsic length scale (ξ) and time scale (η) on the temperature variation (θ) in the semiconductor medium. At $r = 1$, the temperature remains constant at 1.0013015, indicating negligible influence of ξ and η near the gap surface. As r increases, higher values of ξ and η cause a more pronounced temperature reduction, reflecting stronger nonlocal effects. For instance, at $\xi = 1.4$, the temperature decreases from 0.539848 for $\xi = 0.000$, $\eta = 0.000$ to 0.431879 for $\xi = 0.006$, $\eta = 0.005$. This trend reflects the nonlocal effects introduced by the intrinsic length and time scales, which tend to moderate the temperature distribution by accounting for long-range interactions and memory effects. The combined increase in ξ and η results in a more pronounced thermal attenuation.

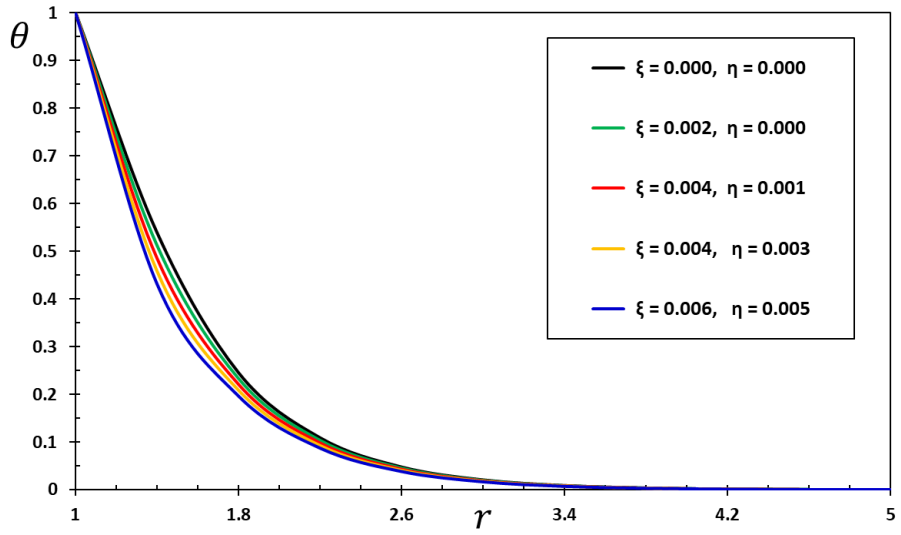

Figure 7. Temperature variation (θ) for various length and time scale parameters.

This trend is sustained at intermediate distances, such as $r = 2.2$ and $r = 3$, where the temperature gradually decreases due to enhanced thermal dissipation driven by nonlocal effects. These results suggest that the nonlocal effects become more pronounced as the distance increases, leading to a gradual reduction in temperature. The interplay between ξ and η enhances the dissipation of thermal energy, likely reflecting the role of spatial and temporal nonlocality in redistributing heat. However, at larger distances ($r = 4.6$ and $r = 5$), the differences between parameter configurations narrow, and the influence of ξ and η diminishes, leading to converging temperature values. While the impact of nonlocal parameters is present, it diminishes as the radial distance grows, indicating that their influence weakens in far-field regions, possibly due to the diminishing contribution of nonlocal interactions.

In conclusion, ξ and η significantly affect temperature variation (θ) at medium distances by introducing size-dependent and time-delayed effects, while their impact weakens at greater distances. Thus, incorporating these parameters is crucial for accurately modeling the thermal behavior of semiconductor materials.

The numerical results in Figure 8 illustrate the variation in the radial displacement field (u) within a semiconductor medium under the influence of changing intrinsic length scale (ξ) and time scale (η). At $r = 1$, the displacement u is highest, starting at 0.864326 for $\xi = 0.000$, $\eta = 0.000$ and progressively decreasing to 0.691461 for $\xi = 0.006$, $\eta = 0.005$. This significant reduction indicates the strong effect of nonlocal parameters near the medium's origin, where long-range interactions and memory effects are most pronounced. As r increases, the influence of ξ and η on displacement u gradually diminishes, though the reduction in u persists. For example, at $r = 1.8$, the displacement u decreases from 0.152534 for $\xi = 0.000$, $\eta = 0.000$ to 0.122027 for $\xi = 0.006$, $\eta = 0.005$. Similarly, at $r = 2.6$, the displacement u reduces from 0.0163456 to 0.0130765 across the same parameter range. This trend reflects the moderation of displacement u as nonlocal effects dissipate with distance.

Also, at greater radial distances (e.g., $r = 4.6$ and $r = 5$), the displacement values become exceedingly small, and differences between parameter configurations narrow further. For instance, at $r = 5$, the displacement u decreases from 1.89E-05 for $\xi = 0.000$, $\eta = 0.000$ to 1.51037E-05 for $\xi = 0.006$, $\eta = 0.005$. This convergence suggests that the nonlocal interactions have a minimal effect on

far-field regions.

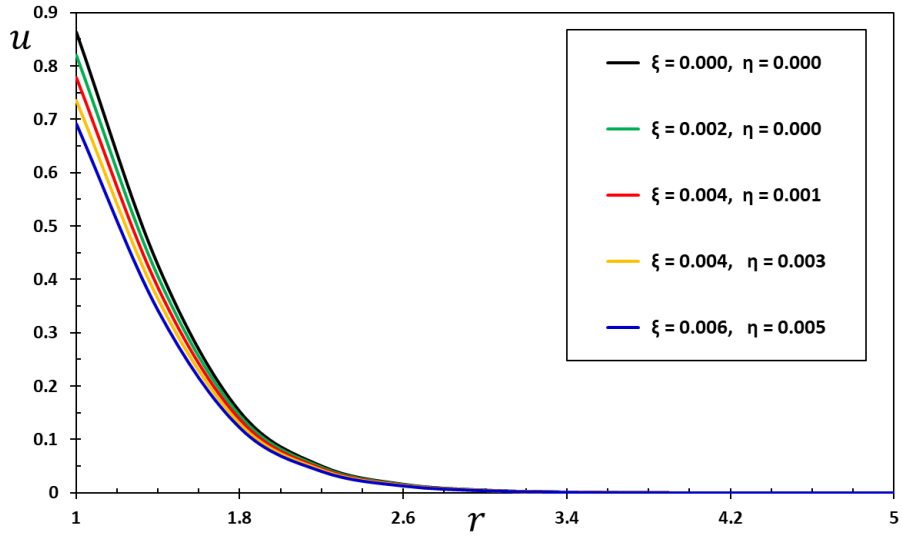

Figure 8. Displacement field (u) for various length and time scale parameters.

Consequently, the intrinsic length scale (ξ) and time scale (η) significantly influence the radial displacement field (u) at smaller and medium distances, introducing size-dependent and time-delayed effects. However, their impact weakens at larger distances, leading to nearly uniform displacement values. These findings highlight the critical role of nonlocal parameters in accurately capturing the mechanical behavior of semiconductor materials.

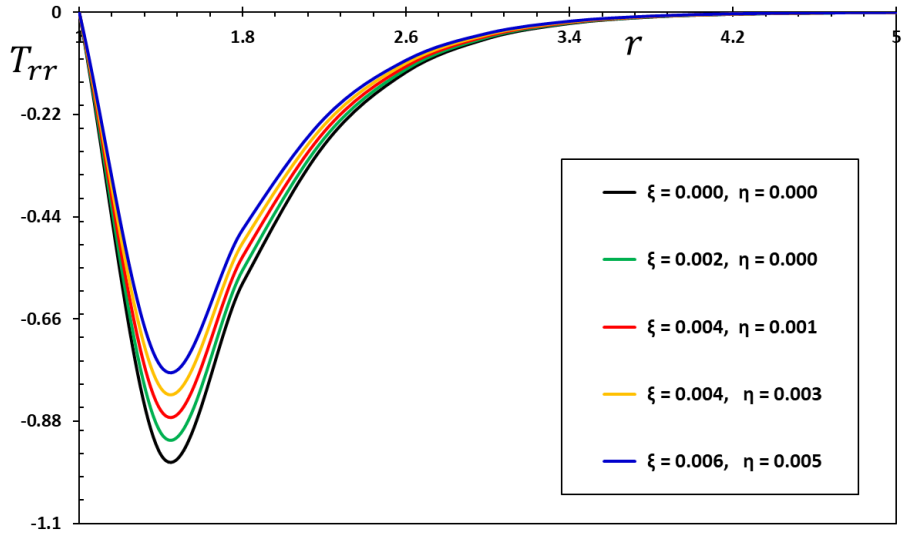

Figure 9. Nonlocal radial thermal stresses (T_{rr}) for various length and time scale parameters.

The numerical results depicted in Figure 9 reflect the variation in radial nonlocal thermal stresses (T_{rr}) within a semiconductor medium, emphasizing the impact of the intrinsic length scale (ξ) and

time scale (η). Notably, at a radius of r = 1, thermal stress remains at zero across all configurations. This indicates that, at the gap surface, the nonlocal parameters do not influence the thermal stress (T_{rr}) at this specific point.

As we move to greater radial distances, the effects of ξ and η become increasingly prominent. At r = 1.4, the thermal stress (T_{rr}) demonstrates a significant reduction, dropping from -0.952456 when both ξ and η are zero, to -0.761965 when set to ξ = 0.006 and η = 0.005. This notable decrease highlights the size-dependent and time-delayed influences introduced by the nonlocal parameters, which serve to alleviate the thermal stress distribution (T_{rr}) within the material. This trend persists at intermediate distances, such as r = 2.2 and r = 3. For instance, at r = 2.2, the thermal stress decreases from -0.285536 to -0.228429 as ξ and η are increased. Similarly, at r = 3, there is a drop from -0.0567629 to -0.0454104. These consistent reductions indicate that as the radial distance increases, the cumulative nonlocal effects of ξ and η continue to effectively moderate the radial thermal stresses (T_{rr}) in the semiconductor.

At larger distances, specifically at r = 4.6 and r = 5, the thermal stress (T_{rr}) values shrink significantly, and the discrepancies across the different configurations narrow even further. For example, at r = 5, the stress value declines from -0.000831434 with ξ = 0.000 and η = 0.000 to -0.000665147 for ξ = 0.006 and η = 0.005. This convergence at extensive radial distances implies that the effects of nonlocal parameters tend to diminish as one moves further away, indicating a reduced sensitivity of thermal stresses to size-dependent and time-delayed phenomena.

In conclusion, the observations affirm that both the intrinsic length scale (ξ) and time scale (η) play critical roles in shaping radial nonlocal thermal stresses (T_{rr}) at smaller and intermediate radial distances, effectively reducing stress magnitudes through their nonlocal effects. Nevertheless, their influence diminishes at larger distances, leading to a convergence of stress values. These findings underscore the crucial importance of integrating ξ and η into models to accurately capture the thermal stress behavior in semiconductor materials.

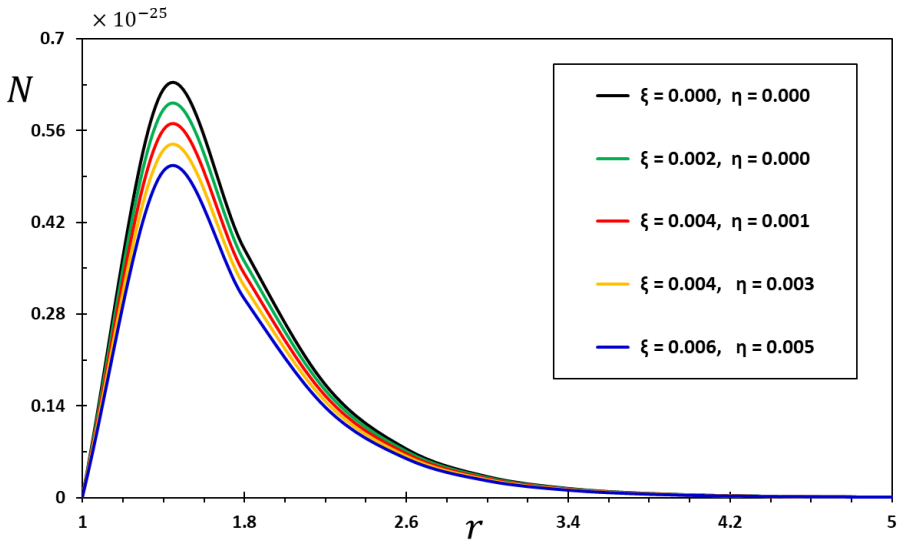

Figure 10. Carrier density (N)for various length and time scale parameters.

The numerical results displayed in Figure 10 illustrate the variation in carrier density (N) within

a semiconductor medium as it responds to nonlocal parameters, namely the intrinsic length scale (ξ) and time scale (η). These parameters play a crucial role in determining the behavior of carrier density (N) across different radial distances. as noticed in Figure 10, at a radius of r = 1, we observe that the carrier density starts at 0.00162501 for the condition where ξ and η are both zero. As the values shift to ξ = 0.006 and η = 0.005, the density (N) drops to 0.00130001. This notable reduction underscores the substantial impact of nonlocal effects, reflecting the underlying size-dependent and time-delayed interactions even in proximity to the origin.

Moving to intermediate distances such as r = 1.8 and r = 2.2, the trend of decreasing carrier density (N) continues as both ξ and η increase. For r = 1.8, the carrier density decreases from 0.379399 (when both parameters are at zero) to 0.303519 for ξ = 0.006 and η = 0.005. Similarly, at r = 2.2, we see a decline from 0.172419 to 0.137935 across the same parameter range. These observations highlight the moderate influence that nonlocal parameters exert on carrier density (N) as the radial distance increases, likely due to enhanced redistribution effects linked to the scaling factors ξ and η.

It can be seen from Figure 10 that at larger radial distances, particularly at r = 3.8 and beyond, the carrier density (N) diminishes noticeably, and the differences between configurations become even less pronounced. For instance, at r = 5, the carrier density decreases from 0.0005704 for ξ = 0.000, η = 0.000 to 0.00045632 for ξ = 0.006, η = 0.005. This convergence suggests that the influence of nonlocal parameters significantly wanes in far-field regions, resulting in carrier density levels that trend toward insignificance.

Accordingly, the intrinsic length scale (ξ) and time scale (η) significantly contribute to the reduction of carrier density (N) within the semiconductor medium, especially at smaller and intermediate distances. These nonlocal parameters account for the size-dependent and time-delayed effects that lead to a gradual decline in N as ξ and η are increased. However, their influence diminishes at larger distances, culminating in nearly convergent values for carrier density (N). These findings emphasize the critical importance of incorporating nonlocal parameters into models to accurately depict carrier transport in semiconductor materials.

8. Conclusions

We introduce the Nonlocal Moore-Gibson-Thompson Photothermal (NMGTPT) Theory, an innovative framework that brings together spatial and temporal nonlocality to address the shortcomings of both traditional and contemporary thermoelastic models. This theory is tailored for semiconductor materials that exhibit microstructural effects, memory-related behavior, and phenomena driven by photo-excitation. The major conclusions and results of this research are summarized as follows:

• In contrast to classical thermoelastic models, the NMGTPT theory integrates both spatial and temporal nonlocality, which allows for a more precise depiction of long-range interactions and memory effects in semiconductor materials.

• The introduction of the MGT thermal relaxation coefficient rectifies the unrealistic notion of infinite heat propagation speed found in classical thermoelasticity, ensuring a thermal response that has finite speed.

• Utilizing the AB fractional derivative significantly improves the model's capability to account for nonlocal and hereditary effects, making it especially suitable for materials that exhibit pronounced memory characteristics.

• The NMGTPT theory uniquely marries photothermal and photoacoustic processes, enabling a holistic examination of photo-induced free carrier dynamics, heat propagation, and mechanical wave movement within semiconductors.

• By integrating an internal length scale, the NMGTPT model adeptly captures size-dependent phenomena, rendering it exceptionally relevant for nanostructured materials, thin films, and micro-scale composites.

• The study assesses the impacts of C and AB fractional derivatives, revealing that AB-derived models yield smoother and more realistic responses, whereas Caputo-based models demonstrate sharper transient behavior.

• The NMGTPT model surpasses traditional frameworks by accurately forecasting stress distribution, thermal diffusion, and carrier transport in semiconductor devices and optoelectronic applications.

Despite its advancements, the NMGTPT model has limitations that need further investigation. The inclusion of nonlocal interactions and fractional derivatives increases computational complexity, requiring advanced numerical methods. It also relies on parameters that are not easily obtainable from experiments, highlighting the need for further validation and calibration. While theoretically robust, its accuracy in real-world applications remains unverified without experimental testing in semiconductor materials. Additionally, its assumption of linear thermoelastic behavior limits its applicability to nonlinear and multi-phase systems, posing a challenge for future development.

To enhance the NMGTPT model, future research should focus on experimental validation to determine nonlocal and fractional parameters, extend the model to nonlinear and multi-scale frameworks for complex interactions, and develop efficient numerical methods like finite element and machine learning approaches. Applications in nanoelectronics, flexible electronics, MEMS/NEMS devices, and quantum materials should be explored, alongside integrating electromagnetic interactions to broaden its use in photonic and optoelectronic systems.

Author contributions

Mofareh Alhazmi: Conceptualization, Methodology, Supervision, Validation, Visualization, Funding acquisition, Resources; Ahmed E. Abouelregal: Formal analysis, Investigation, Software, Data Curation, Writing—original draft preparation, Visualization, Writing—review and editing. All authors have read and approved the final version of the manuscript and contributed equally to the development of this study.

Use of Generative-AI tools declaration

The authors declare they have not used Artificial Intelligence (AI) tools in the creation of this article.

Acknowledgments

This research is funded by the Deanship of Graduate Studies and Scientific Research at Jouf University through the Fast-Track Research Funding Program.

Conflict of interest

The authors declared no potential conflicts of interest with respect to the research, authorship and publication of this article.

References

1. E. Gutiérrez-Reyes, C. García-Segundo, A. García-valenzuela, R. Ortega, C. Buj, F. Filbir, Heat transport considerations in the mathematical analysis of the photoacoustic and photothermal effects, *J. Phys. Commun*., **3** (2019), 085007. https://doi.org/10.1088/2399-6528/ab376d
2. J. Zakrzewski, M. Pawlak, O. Matsuda, D. Todorovic, J. Liu, Semiconductor physics: Plasma, thermal, elastic, and acoustic phenomena, *J. Appl. Phys*., **136** (2024), 120401. https://doi.org/10.1063/5.0234837
3. K. Lotfy, I. S. Elshazly, B. Halouani, P. Ailawalia, A. A. El-Bary, Photo-thermo-acoustic waves interaction for nanostructured rotational semiconductor material subjected to laser pulse, *Eur. Phys. J. B*, **97** (2024), 189. https://doi.org/10.1140/epjb/s10051-024-00830-0
4. A. R. Warrier, K. P. Vijayakumar, Photothermal studies in semiconductor materials, In: *Photoacoustic Photothermal Spectrosc*, Elsevier, 2023, 245–26.
5. S. Galovic, K. Djordjevic, M. Dragas, D. Milicevic, E. Suljovrujic, Dynamics of photoinduced charge carrier and photothermal effect in pulse-illuminated narrow gap and moderate doped semiconductors, *Mathematics*, **13** (2025), 258. https://doi.org/10.3390/math13020258
6. A. E. Abouelregal, H. M. Sedighi, A. H. Sofiyev, Modeling photoexcited carrier interactions in a solid sphere of a semiconductor material based on the photothermal Moore–Gibson–Thompson model, *Appl. Phys. A*, **127** (2021), 845. https://doi.org/10.1007/s00339-021-04971-2
7. B. Feng, A. Mo, W. Dong, W. Fan, J. Ren, Z. Li, et al., Investigation into the carrier recombination in Sb2Se3: Photo thermal effect, trapped carrier absorption and hot carrier cooling, *Chem. Phys*., **588** (2025), 112448. https://doi.org/10.1016/j.chemphys.2024.112448
8. V. D. Kupradze, *Three-dimensional problems of elasticity and thermoelasticity*, Elsevier, 2012.
9. C. Truesdell, *Linear theories of elasticity and thermoelasticity: Linear and nonlinear theories of rods, plates, and shells*, Springer, 2013.
10. S. L. Guo, Y. X. Zhang, K. F. Wang, B. L. Wang, C. W. Zhang, Effects of non-Fourier heat conduction and surface heating rate on thermoelastic waves in semi-infinite ceramics subject to thermal shock, *Ceram. Int*., **47** (2021), 17494–17501. https://doi.org/10.1016/j.ceramint.2021.03.067
11. G. A. Maugin, A. Berezovski, Material formulation of finite-strain thermoelasticity and applications, *J. Therm. Stresses*, **22** (1999), 421–449. https://doi.org/10.1080/014957399280823
12. J. Gawinecki, Initial-boundary value problems in linear and nonlinear hyperbolic thermoelasticity theory, Z. *Angew. Math. Mech*. **78** (1998), 911–912. https://doi.org/10.1002/zamm.19980781528
13. R. F. Silva, P. G. Coelho, F. M. Conde, C. J. Almeida, A. L. Custódio, Topology optimization of thermoelastic structures with single and functionally graded materials exploring energy and stress-based formulations, *Struct. Multidisc. Optim*., **68** (2025), 11. https://doi.org/10.1007/s00158-024-03929-1
14. A. E. Green, P. Naghdi, A re-examination of the basic postulates of thermomechanics, *Proc. R. Soc. Lond. A*, **432** (1991), 171–194. https://doi.org/10.1098/rspa.1991.0012

15. A. E. Green, P. Naghdi, On undamped heat waves in an elastic solid, *J. Therm. Stresses*, **15** (1992), 253–264. https://doi.org/10.1080/01495739208946136
16. A. E. Green, P. Naghdi, Thermoelasticity without energy dissipation, *J. Elast*., **31** (1993), 189–208. https://doi.org/10.1007/BF00044969
17. R. Quintanilla, Moore–Gibson–Thompson thermoelasticity, *Math. Mech. Solids*, **24** (2019), 4020–4031. https://doi.org/10.1177/1081286519862007
18. R. Quintanilla, Moore-Gibson-Thompson thermoelasticity with two temperatures, *Appl. Eng. Sci.*, **1** (2020), 100006. https://doi.org/10.1016/j.apples.2020.100006
19. C. Cattaneo, A form of heat-conduction equations which eliminates the paradox of instantaneous propagation, *C. R. Acad. Sci*., **247** (1958), 431. https://ci.nii.ac.jp/naid/10018112216
20. P. Vernotte, Some possible complications in the phenomena of thermal conduction, *C. R. Acad. Sci*., **252** (1961), 2190–2191.
21. A. E. Abouelregal, M. Marin, A. Foul, S. S. Askar, Thermoviscoelastic responses in Kirchhoff circular micro-plate via MGT thermoelastic model and modified couple stress theory, *Mech. Solids*, **59** (2024), 2269–2291. https://doi.org/10.1134/S002565442460449X
22. A. E. Abouelregal, Generalized thermoelastic MGT model for a functionally graded heterogeneous unbounded medium containing a spherical hole, *Eur. Phys. J. Plus*, **137** (2022), 953. https://doi.org/10.1140/epjp/s13360-022-03160-1
23. A. E. Abouelregal, M. Alesemi, Evaluation of the thermal and mechanical waves in anisotropic fiber-reinforced magnetic viscoelastic solid with temperature-dependent properties using the MGT thermoelastic model, *Case Stud. Therm. Eng*., **36** (2022), 102187. https://doi.org/10.1016/j.csite.2022.102187
24. A. E. Abouelregal, H. M. Sedighi, S. F. Megahid, Photothermal-induced interactions in a semiconductor solid with a cylindrical gap due to laser pulse duration using a fractional MGT heat conduction model, *Arch. Appl. Mech.*, **93** (2023), 2287–2305. https://doi.org/10.1007/s00419-023-02383-7
25. F. K. Moore, W. E. Gibson, Propagation of weak disturbances in a gas subject to relaxation effects, *J. Aerosp. Sci*., **27** (1960), 117–127. https://doi.org/10.2514/8.8418
26. P. A. Thompson, A. A. Sonin, Compressible-fluid dynamics, *Phys. Today*, **26** (1973), 65–69. https://doi.org/10.1063/1.3127987
27. R. Barretta, F. Marotti de Sciarra, M. Concurrent S. Vaccaro, Nonlocal elasticity for nanostructures: A review of recent achievements, *Encyclopedia*, **3** (2023), 279–310. https://doi.org/10.3390/encyclopedia3010018
28. E. Kröner, Elasticity theory of materials with long range cohesive forces, *Int. J. Solids Struct*., **3** (1967), 731–742. https://doi.org/10.1016/0020-7683(67)90049-2
29. K. Duan, L. Li, Y. Hu, X. Wang, Enhanced interfacial strength of carbon nanotube/copper nanocomposites via Ni-coating: Molecular-dynamics insights, *Physica E*, **88** (2017), 259–264. https://doi.org/10.1016/j.physe.2017.01.015
30. A. C. Eringen, Linear theory of nonlocal elasticity and dispersion of plane waves, *Int. J. Eng. Sci*., **10** (1972), 425–435. https://doi.org/10.1016/0020-7225(72)90050-X
31. A. C. Eringen, On differential equations of nonlocal elasticity and solutions of screw dislocation and surface waves, *J. Appl. Phys*., **54** (1983), 4703–4710. https://doi.org/10.1063/1.332803

32. G. Romano, R. Barretta, Stress-driven versus strain-driven nonlocal integral model for elastic nano-beams, *Compos. B Eng.*, **114** (2017), 184–188. https://doi.org/10.1016/j.compositesb.2017.01.008
33. S. Li, W. Zheng, L. Li, Spatiotemporally nonlocal homogenization method for viscoelastic porous metamaterial structures, *Int. J. Mech. Sci.*, **282** (2024), 109572. https://doi.org/10.1016/j.ijmecsci.2024.109572
34. Y. Jiang, L. Li, Y. Hu, A spatiotemporally-nonlocal continuum field theory of polymer networks, *Sci. China Phys. Mech. Astron.*, **66** (2023), 254611. https://doi.org/10.1007/s11433-022-2053-1
35. A. E. Abouelregal, M. Marin, A. Öchsner, A modified spatiotemporal nonlocal thermoelasticity theory with higher-order phase delays for a viscoelastic micropolar medium exposed to short-pulse laser excitation, *Continuum Mech. Thermodyn.*, **37** (2025), 15. https://doi.org/10.1007/s00161-024-01342-z
36. A. E. Abouelregal, M. Marin, Y. Alhassan, D. Atta, A novel space–time nonlocal thermo-viscoelastic model with two-phase lags for analyzing heat diffusion in a half-space subjected to a heat source, *Iran. J. Sci. Technol. Trans. Mech. Eng.*, 2025. https://doi.org/10.1007/s40997-025-00835-9
37. S. El-Sapa, K. Lotfy, E. S. Elidy, A. El-Bary, R. S. Tantawi, Photothermal excitation process in semiconductor materials under the effect moisture diffusivity, *Silicon*, **15** (2023), 4171–4182. https://doi.org/10.1007/s12633-023-02311-y
38. S. El-Sapa, A. A. Almoneef, K. Lotfy, A. A. El-Bary, A. M. Saeed, Moore-Gibson-Thompson theory of a non-local excited semiconductor medium with stability studies, *Alex. Eng. J.*, **61** (2022), 11753–11764. https://doi.org/10.1016/j.aej.2022.05.036
39. S. El-Sapa, N. Becheikh, H. Chtioui, K. Lotfy, M. A. Seddeek, A. A. El-Bary, et al., Moore–Gibson–Thompson model with the influence of moisture diffusivity of semiconductor materials during photothermal excitation, *Front. Phys.*, **11** (2023), 1224326. https://doi.org/10.3389/fphy.2023.1224326
40. Y. Q. Song, J. T. Bai, Z. Y. Ren, Study on the reflection of photothermal waves in a semiconducting medium under generalized thermoelastic theory, *Acta Mech.*, **223** (2012), 1545–1557. https://doi.org/10.1007/s00707-012-0677-1
41. D. M. Todorović, Plasma, thermal, and elastic waves in semiconductors, *Rev. Sci. Instrum.*, **74** (2003), 582–585. https://doi.org/10.1063/1.1523133
42. W. Nowacki, *Thermoelasticity*, Elsevier, 2013.
43. B. Audoin, H. Meri, C. Rossignol, Two-dimensional diffraction of plasma, thermal, and elastic waves generated by an infrared laser pulse in semiconductors*, Phys. Rev. B*, **74** (2006), 214304. https://doi.org/10.1103/PhysRevB.74.214304
44. R. B. Hetnarski, J. Ignaczak, Generalized thermoelasticity, *J. Therm. Stresses*, **22** (1999), 451–476. https://doi.org/10.1080/014957399280832
45. A. E. Abouelregal, M. A. Fahmy, Generalized Moore-Gibson-Thompson thermoelastic fractional derivative model without singular kernels for an infinite orthotropic thermoelastic body with temperature-dependent properties, *ZAMM-J. Appl. Math. Mech.*, **102** (2022), e202100533. https://doi.org/10.1002/zamm.202100533

46. A. E. Abouelregal, Y. Alhassan, S. S. Alsaeed, M. Marin, M. E. Elzayady, MGT photothermal model incorporating a generalized Caputo fractional derivative with a tempering parameter: Application to an unbounded semiconductor medium, *Contemp. Math*., **5** (2024), 6556–6581. https://doi.org/10.37256/cm.5420245963
47. J. A. Tenreiro Machado, M. F. Silva, R. S. Barbosa, I. S. Jesus, C. M. Reis, M. G. Marcos, et al., Some applications of fractional calculus in engineering, *Math. Probl. Eng*., **2010** (2010), 639801, https://doi.org/10.1155/2010/639801
48. M. Caputo, F. Mainardi, A new dissipation model based on memory mechanism, *Pure Appl. Geophys*., **91** (1971), 134–147. https://doi.org/10.1007/BF00879562
49. M. Caputo, M. Fabrizio, A new definition of fractional derivative without singular kernel, *Prog. Fract. Differ. Appl*., **1** (2015), 73–85. http://doi.org/10.12785/pfda/010201
50. A. Atangana, D. Baleanu, New fractional derivatives with nonlocal and non-singular kernel: Theory and application to heat transfer model, *Therm. Sci*., **20** (2016), 763–769. https://doi.org/10.2298/TSCI160111018A
51. M. Lazar, E. Agiasofitou, Nonlocal elasticity of Klein–Gordon type: Fundamentals and wave propagation, *Wave Motion*, **114** (2022), 103038. https://doi.org/10.1016/j.wavemoti.2022.103038
52. E. Agiasofitou, M. Lazar, Nonlocal elasticity of Klein-Gordon type with internal length and time scales: Constitutive modelling and dispersion relations, *PAMM*, **23** (2023), e202300065. https://doi.org/10.1002/pamm.202300065
53. F. Ebrahimi, K. Khosravi, A. Dabbagh, Wave dispersion in viscoelastic FG nanobeams via a novel spatial–temporal nonlocal strain gradient framework, *Waves Random Complex Media*, **34** (2024), 2962–2984. https://doi.org/10.1080/17455030.2021.1970282
54. F. Ebrahimi, K. Khosravi, A. Dabbagh, A novel spatial–temporal nonlocal strain gradient theorem for wave dispersion characteristics of FGM nanoplates, *Waves Random Complex Media*, **34** (2024), 3490–3509. https://doi.org/10.1080/17455030.2021.1979272
55. R. G. Jacquot, J. W. Steadman, C. N. Rhodine, The Gaver-Stehfest algorithm for approximate inversion of Laplace transforms, *IEEE Circuits Syst. Mag*., **5** (1983), 4–8.
56. A. Kuznetsov, On the convergence of the Gaver-Stehfest algorithm, *SIAM J. Numer. Anal*., **51** (2013), 2984–2998. https://doi.org/10.1137/13091974X
57. A. Sur, Photo-thermoelastic interaction in a semiconductor with cylindrical cavity due to memory-effect, *Mech. Time-Depend. Mater*., **28** (2024), 1219–1243. https://doi.org/10.1007/s11043-023-09637-5

AIMS Press